

CMUG CCI+ Deliverable

Reference: Final report WP5.5: Cloud and Aerosol Analysis Study
Due date: August 2024
Submission date: September 2024
Version: 0.4



Climate Modelling User Group

Deliverable D3.1e

Final report WP5.5: Cloud and Aerosol Analysis Study

Centres providing input: ECMWF, BSC

Version nr.	Date	Status
0.1	03 September 2024	First draft of WP5.5.1
0.2	25 September 2024	First draft of WP5.5.2
0.3	26 September 2024	Submitted to CMUG PI
0.4	02 October 2024	Resubmission to CMUG PI

CMUG CCI+ Deliverable

Reference: Final report WP5.5: Cloud and Aerosol Analysis Study
Due date: August 2024
Submission date: September 2024
Version: 0.4



CMUG CCI+ Deliverable D3.1e

Final report in WP5.5

Table of Contents

1. Purpose and scope of this report	3
2. WP5.5.1: Dust aerosol analysis in the BSC system	4
Preliminary work and overview	4
2.1. <i>D2.0e WP5.5.1 summary: assimilation of SLSTR AOD</i>	4
2.2. <i>Sensitivity and investigation on the uncertainties over ocean</i>	9
Diagnosing inflation factors of the observational error covariance matrix.....	9
Design of experiments for best use of uncertainty estimates of AOD	10
Estimate of R inflation factor	11
Results of the sensitivity experiments	13
Diagnostics for the experiment with inflation of uncertainties over ocean.....	20
Summary and recommendations.....	21
3. WP5.5.2 Cloud/Aerosol analysis with the ECMWF system	23
Aim	23
Summary of the technical preparations	23
Observation operator for AODs	25
Observation operator for CODs	25
Designing quality control and observation errors	26
Impact assessment in depleted observing system	30
Impact assessment in full observing system.....	34
Conclusions and recommendations.....	35
References	39



Final report on progress achieved in WP5.5

1. Purpose and scope of this report

This document is the final report on activities carried on in the WP5.5 Clouds and Aerosol study CMUG-CCI+. The aim of the study is to exploit ESA CCI and CCI+ data of aerosols and clouds for assimilation in Earth System Models. For this purpose, we use two ECVs, clouds and aerosols, and two different models and approaches for the assimilation. ECMWF assimilates operationally, in their 4D-Var system, aerosol optical depth in the Copernicus Atmosphere Monitoring Service for atmospheric composition forecasts, while limited cloud information is assimilated for Numerical Weather Prediction and reanalyses. This study proposes to assimilate both, aerosols and cloud information synergistically in the 4D-Var system.

BSC produces operationally daily forecasts of dust for the WMO Barcelona Dust Regional Centre. It expects to produce forecasts with dust assimilation with an ensemble LETKF assimilation scheme in the next model upgrade, scheduled for Q2 of next year. Dedicated dust observations are essential for this application, as well as for the constraint of the dust cycle in the Earth system. Using satellite dust optical depth, the MONARCH model at BSC has produced a 10-years dust reanalysis (Di Tomaso et al. 2022), which has been recently extended for two more years. This work will assess the potential benefit of using most recent developments on CCI aerosol retrievals for dust data assimilation, with perspectives of being used for assimilation in future dust reanalysis, and for verification of past operational forecasts.

CMUG CCI+ Deliverable

Reference: Final report WP5.5: Cloud and Aerosol Analysis Study
Due date: August 2024
Submission date: September 2024
Version: 0.4



2. WP5.5.1: Dust aerosol analysis in the BSC system

Lead partner: BSC

Authors: Jeronimo Escribano, Eleni Karnezi, Emanuele Emili and Calum Meikle

Preliminary work and overview

The CMUG study follows up part of the work performed during the ESA's DOMOS project. During DOMOS, three experiments were performed: (i) assimilation of aerosol optical depth (AOD) from VIIRS Deep Blue, version 1 from Suomi-NPP (SNPP), filtered by retrieval flag of "dust"; (ii) Assimilation of dust extinction coefficient from the LIVAS product, based on CALIOP profiles, and (iii) joint assimilation of LIVAS and VIIRS data. Hence, WP5.5.1 experiments can be directly compared to those of DOMOS. This allows to fully exploit their outcomes and sets a baseline for the evaluation of WP5.5.1 results. That said, this task explores the assimilation of CCI data for the same case of study and using the same verifications scores and tools.

WP5.5.1 assimilates the v1.14 of SLSTR aerosol optical depth, produced by Swansea University, during the Godzilla dust event in June 2020. The data was kindly shared by Peter North and Kevin Pearson for this study.

A large part of the 5.5.1 work was documented in D2.0e (Interim Report). We have shown in D2.0e the results of assimilating SLSTR AOD with the following main outcomes:

- (i) Coarse AOD and Dust AOD products from SLSTR v1.14 retrievals underestimate the strength of the dust event, in comparison with other observational sources of information. Therefore, we decided to assimilate total AOD instead.
- (ii) The assimilation of AOD from SLSTR improves significantly the forecasts and the analyses of dust AOD.
- (iii) The assumption of a linear model for the observational uncertainties might produce dust analysis of similar quality to those of the assimilation of the ESA's DOMOS project (VIIRS, LIVAS).
- (iv) The analysis that uses the pixelwise uncertainty of AOD provided in the SLSTR retrieval might overfit the observations in the data assimilation procedure, due to a possible underestimation of the uncertainty over ocean.

Novel work was added to this report, with focus in point (iv). We re-run the assimilation experiments, estimate the uncertainties and provide a simple evaluation of the experiments.

In order to provide a self-consistent document, we will briefly summarize D2.0e in the next Section and we will extend it with the new results.

2.1. *D2.0e WP5.5.1 summary: assimilation of SLSTR AOD*



In D2.0e we have compared SLSTR AOD, SLSTR coarse AOD (computed by subtracting fine AOD to the total AOD retrievals), dust optical depth (DOD) of the MONARCH control simulation, the VIIRS-SNPP Deep Blue v1 coarse DOD over land (following Pu and Ginoux, 2016), and the VIIRS dust-filtered AOD used in ESA’s DOMOS project. We have shown that both, coarse AOD and dust AOD from SLSTR underestimate considerably the “Godzilla” dust plume in June 2020. Figure 1 shows the evolution of satellite and modelled AOD and DOD over the domain and period of interest. It is possible to see the underestimation of SLSTR coarse AOD (5th row) and SLSTR DOD (4th row). Therefore, and as it is explained in D2.0e, we proceed with the assimilation of AOD over the domain because it seems to capture better the dust event and does not exacerbate the negative bias of the model prior.

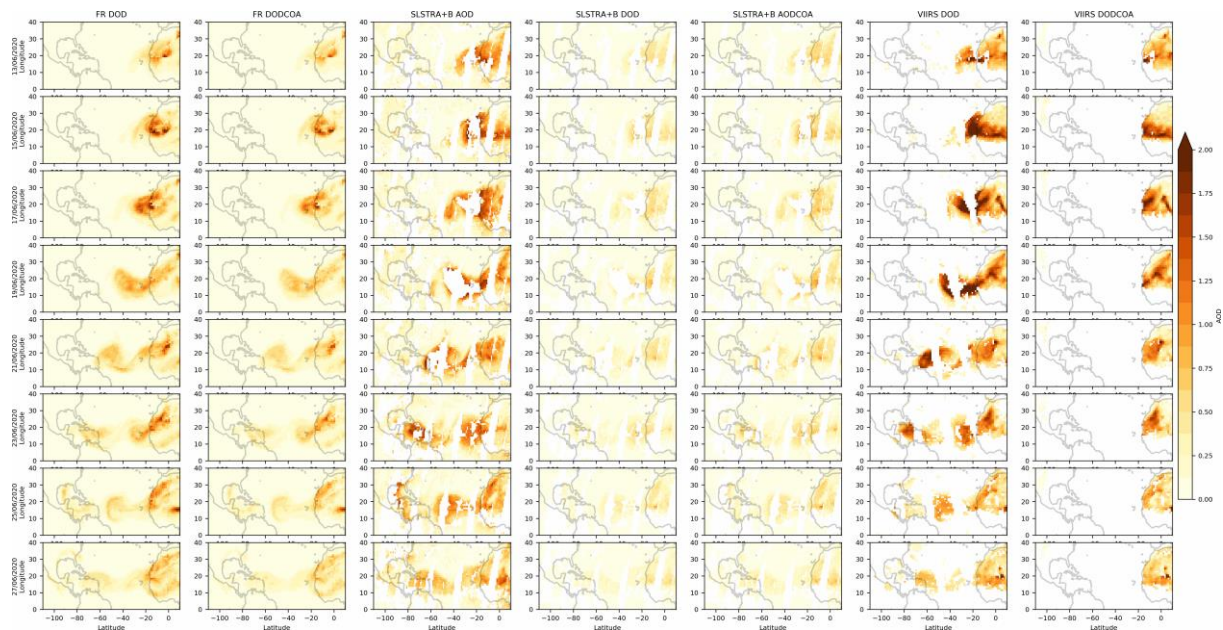


Figure 1: Model and satellite retrievals aerosol information from 18UTC June 13 (top row) to 18UTC June 27(bottom row) in two-day time steps. Columns: Control model run AOD, Control model run coarse AOD, SLSTR AOD, SLSTR dust AOD, SLSTR coarse AOD, VIIRS SNPP dust AOD, VIIRS SNPP coarse Dust AOD.

Data assimilation experiments were performed by using the Local Ensemble Kalman Filter (LETKF, Hunt et al. 2007) coupled to a 20 members ensemble of global MONARCH runs. More details on the MONARCH and LETKF configurations can be found in D2.0e.

We perform two experiments with SLSTR AOD data from Sentinel-3A and Sentinel-3B. The first one assumes a linear model for the AOD uncertainty in the data assimilation by $AOD_{uncertainty} = 0.2 * AOD + 0.05$ (named SLSTR-linear or LIN_UNC in the plots). The second experiment uses the AOD uncertainties provided in the retrieval at the pixel level basis (named SLSTR-px-1 or PIX_UNC1 in the plots). Maps of the experiment analyses are shown in Figure 2, along with the VIIRS experiment produced in the DOMOS project. In this Figure, the system show consistency in decreasing the departures with the assimilated observations. In the same way, it provides similar AOD fields than those of the VIIRS analyses. The experiment



that uses the pixel level uncertainty shows larger AOD values, and a small-scale pattern that it is not found in the other analyses. This might be due an underestimation of the uncertainties in the data assimilation, that will be discussed later in this report.

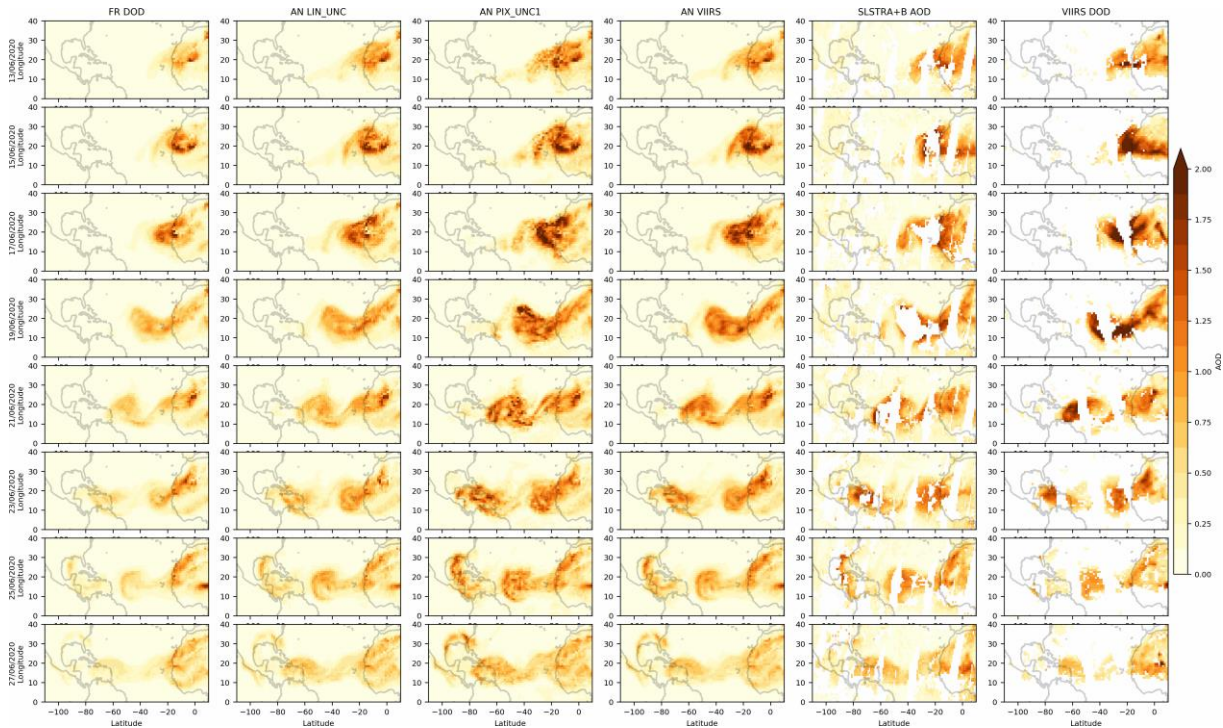


Figure 2: Assimilation of SLSTR AOD. Snapshots of simulated (18UTC) dust optical depth and satellite retrievals. Columns: model control run, analysis of the linear uncertainty experiment, analysis of the pixel-level uncertainty, analysis of the VIIRS experiment, averaged SLSTR AOD, averaged SLSTR DOD and VIIRS DOD.

We are interested in assessing the ability of the system to improve DOD forecasts and analyses of this extreme dust event. Although a proper verification is planned in OWP5.5, we provide here quick comparison of MONARCH forecasts and analyses with coarse AOD retrieval from AERONET SDA product. Spatially averaged times series over the selected AERONET sites of Figure 3 are shown in Figure 4 for the forecasts and analyses DOD. In Figure 4 we added the results of two more ESA’s DOMOS experiments, that assimilate the dust extinction coefficient product from LIVAS (Amiridis et al., 2015), and the joint assimilation of LIVAS and VIIRS filtered AOD in the same data assimilation configuration.





Figure 3: AERONET sites used for the verification: La_Parguera, NEON_OSBS, Santa_Cruz_Tenerife, Tudor_Hill, Cape_San_Juan, Guadeloup, Ragged_Point, ARM_Graciosa, Saada, Dakar_Belair, Izana, La_Laguna, and NEON_GUAN.

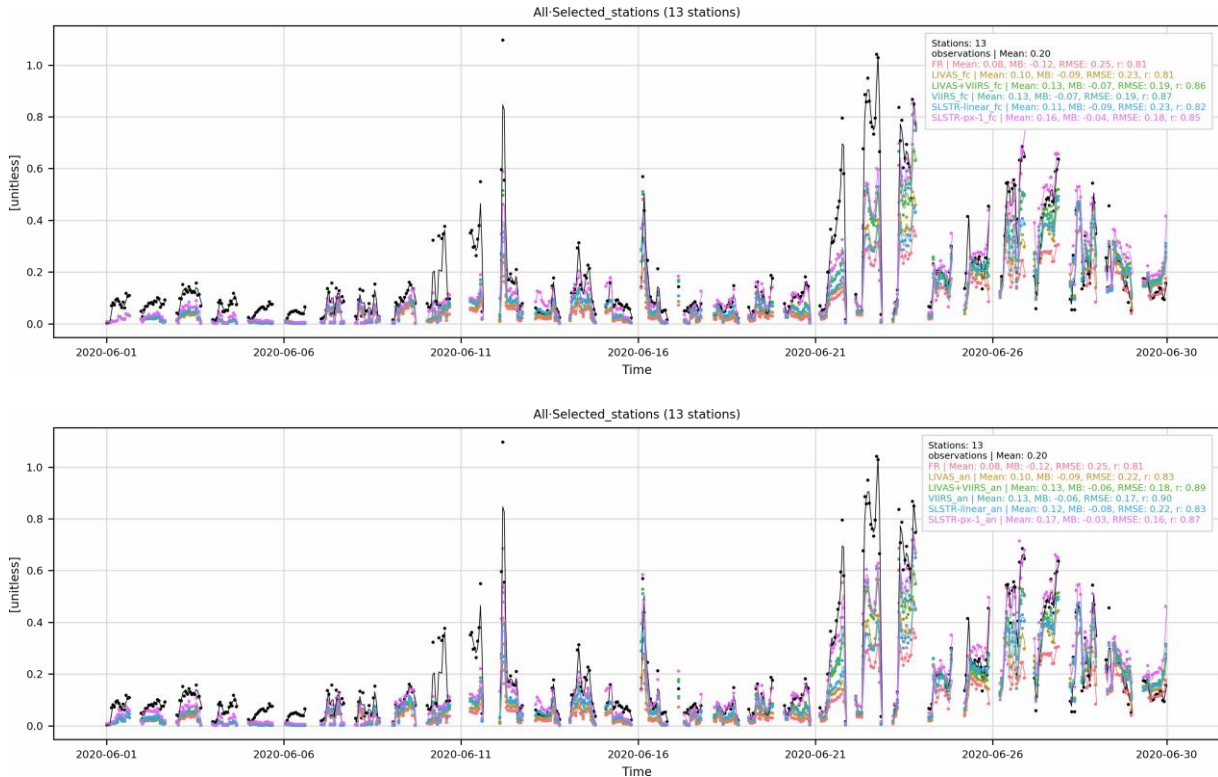


Figure 4: Spatially averaged time-series of coarse AOD AERONET retrievals and MONARCH DOD coarse forecasts (top) and analyses (bottom).

Figure 4 indicates that both, forecasts and analyses of all assimilation experiments improve the bias and show better skills than the control run. Detailed information on the computed scores is presented in Table 1.

	Mean	p50	Std.	MB	NMB	MFB (%)	MAE	NME	MFE (%)	RMSE	r
Obs.	0.20	0.07	0.31	----	----	----	----	----	----	----	----
FR	0.08	0.02	0.12	0.12	59.11	100.06	0.12	63.5	111.75	0.25	0.81

CMUG CCI+ Deliverable

Reference: Final report WP5.5: Cloud and Aerosol Analysis Study
 Due date: August 2024
 Submission date: September 2024
 Version: 0.4



LIVAS_fc	0.10	0.02	0.15	0.09	48.25	-85.38	0.11	57.01	102.93	0.23	0.81
LIVAS_an	0.10	0.03	0.16	0.09	47.23	-84.01	0.11	55.17	101.15	0.22	0.83
LIVAS+VIIRS_fc	0.13	0.03	0.19	0.07	35.63	-69.43	0.09	48.08	93.63	0.19	0.86
LIVAS+VIIRS_an	0.13	0.03	0.20	0.06	33.07	-66.67	0.09	44.86	90.70	0.18	0.89
VIIRS_fc	0.13	0.03	0.20	0.07	34.79	-71.41	0.09	47.37	94.87	0.19	0.87
VIIRS_an	0.13	0.03	0.20	0.06	32.20	-68.90	0.09	43.82	92.17	0.17	0.90
SLSTR-linear_fc	0.11	0.03	0.15	0.09	44.07	-71.05	0.11	54.36	93.66	0.23	0.82
SLSTR-linear_an	0.12	0.04	0.16	0.08	41.37	-66.97	0.10	51.59	90.29	0.22	0.83
SLSTR-px1_fc	0.16	0.05	0.22	0.04	19.18	-39.67	0.09	44.57	79.61	0.18	0.85
SLSTR-px1_an	0.17	0.06	0.23	0.03	15.03	-33.38	0.08	39.87	75.24	0.16	0.87

Table 1: Verification coarse AOD scores for all AERONET sites in the period. Columns show the AOD computed scores: Mean (Mean), median (p50), standard deviation (Std.), mean bias (MB), normalised mean bias (NMB), mean fractional bias (MFB), mean absolute bias (MAE), normalised mean error (NME), mean fractional error (MFE), root mean squared error (RMSE) and Pearson correlation coefficient (r). Data assimilation experiments for forecasts (_fc) and analyses (_an): control run (FR), assimilation of LIVAS (LIVAS), assimilation of LIVAS and VIIRS data (LIVAS+VIIRS_), assimilation of SLSTR assuming linear model for uncertainties (SLSTR_linear_), and assimilation of SLSTR using pixel-level uncertainties (SLSTR_px1_).

Table 1 show quantitative improvements after assimilation for all bias and error scores. As expected, analyses show better skills than forecast. SLSTR-linear experiment slightly worse skills comparable to their VIIRS counterpart bias metrics and most of the error and correlation metrics; but better scores than the LIVAS assimilation. SLSTR-px1 show noticeable better scores than the SLSTR-linear experiment, and also better than most of the DOMOS experiments.

The strong low bias of the control run, and the expected high bias of the SLSTR assimilated observations might play an important role in the better scores of SLSTR-px1 experiment. In this data assimilation experiments, we are assuming that SLSTR AOD can be compared with the model DOD, and thus the assimilation can compensate the low bias of the prior with a high bias of the assimilated observations.

Figure 5 presents SLSTR level2 AOD and AOD uncertainties. It shows that, in comparison with the linear model of uncertainties (diagonal line in the plot), the uncertainties of the SLSTR product have low values over the oceanic dust plume (identified by large AOD over ocean). The bias adjustment mechanism mentioned above, in addition to the possible low uncertainty of the assimilated oceanic AOD in the system might cause an overfit the observations in the assimilation, which can degrade the quality of analyses and forecasts, and might explain the



noise pattern of Figure 2. Next sections of this report will continue by investigating this aspect of the assimilation experiment.

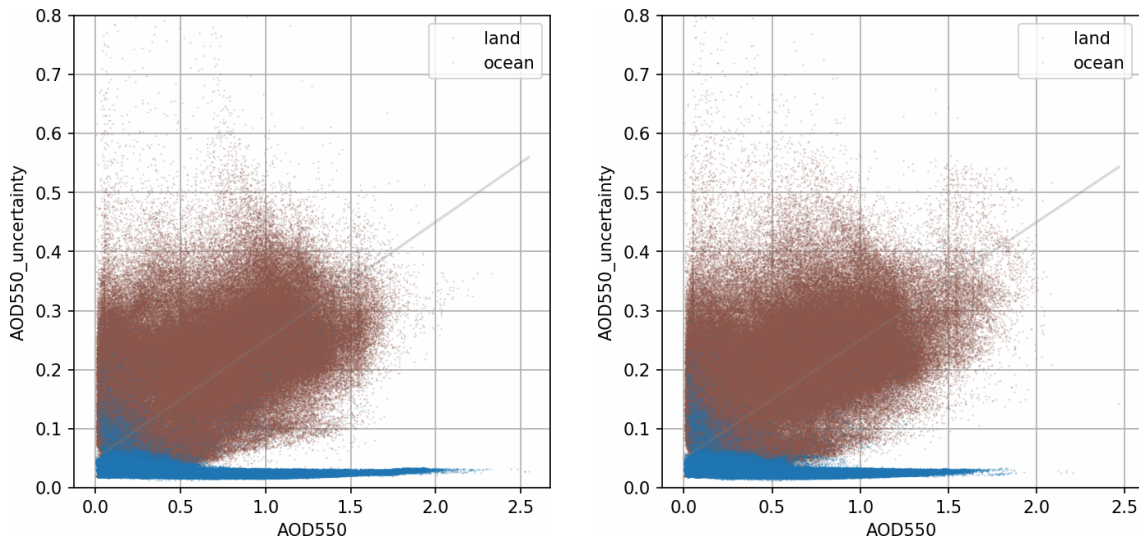


Figure 5: SLSTR AOD550 and associated uncertainties for retrievals between June 12 and June 27. Left column shows retrievals of S3A and right column shows the retrieval of S3B. Blue dots are retrievals over ocean and brown dots are retrievals over land

2.2. Sensitivity and investigation on the uncertainties over ocean

D2.0e report suggests that the uncertainties provided by the SLSTR retrieval over ocean are lower than expected for their use in our data assimilation experiments. Therefore, we propose a new series of experiments to tackle this issue, aiming to elucidate the possible overfitting over ocean, and to provide a better estimate of ocean AOD uncertainties that have to be ingested in the data assimilation system for this dust event.

Diagnosing inflation factors of the observational error covariance matrix

In numerous operational centres estimates of observational errors are diagnosed from the data assimilation statistics. We follow the work by Desroziers et al 2005, implementing part of the diagnostics in the observation space, namely:

$$\begin{aligned}
 E[\mathbf{d}_b^a (\mathbf{d}_b^o)^T] &= \mathbf{H} \mathbf{B} \mathbf{H}^T \quad , \\
 E[\mathbf{d}_b^o (\mathbf{d}_b^o)^T] &= \mathbf{H} \mathbf{B} \mathbf{H}^T + \mathbf{R} \quad , \\
 E[\mathbf{d}_a^o (\mathbf{d}_b^o)^T] &= \mathbf{R} \quad , \\
 E[\mathbf{d}_b^a (\mathbf{d}_a^o)^T] &= \mathbf{H} \mathbf{A} \mathbf{H}^T \quad ,
 \end{aligned}
 \tag{Equation 1}$$



where E is the mathematical expectancy, \mathbf{H} is the linearized observation operator, \mathbf{B} is the covariance matrix of the background errors, \mathbf{R} is the covariance matrix of the observational errors, \mathbf{A} is the covariance matrix of the analysis, T stands for matrix transposition, and the departures between the observations and the simulated forecasts and analyses are computed by:

$$\begin{aligned}\mathbf{d}_b^o &= \mathbf{y} - H(\mathbf{x}^b) \quad , \\ \mathbf{d}_b^a &= H(\mathbf{x}^a) - H(\mathbf{x}^b) \quad , \\ \mathbf{d}_a^o &= \mathbf{y} - H(\mathbf{x}^a) \quad .\end{aligned}$$

with H the observation operator, \mathbf{y} the vector of observations, \mathbf{x}^b the prior and \mathbf{x}^a the analysis.

By construction, these diagnostics are sensitive to biases and the distribution (assumed Gaussian) of the background and observational errors with respect to their true value. In addition, the LETKF has its own additional assumptions, so the strict optimality of the solution (and thus some the diagnostics of Desroziers et al. 2005) are not completely fulfilled in our case. Despite these limitations, these diagnostics are still a valuable tool for examining the error balance in the system.

Diagonals elements from the matrices above are computed with no cost on our LETKF experiments. In practice, the diagonal of $\mathbf{H}\mathbf{B}\mathbf{H}^T$ is the variance of the forecast ensemble AOD, the diagonal of $\mathbf{H}\mathbf{A}\mathbf{H}^T$ is the diagonal of the analysis AOD ensemble and the diagonal of \mathbf{R} is the variance of the observational errors. On the left side, the diagonal of the matrices are difference of the multiplication between the mean ensemble forecasts, analyses and observations. If all hypothesis of the construction of these diagnostics are fulfilled, we can estimate inflation factors for the observational error covariance matrix \mathbf{R} by computing the ratio between the left and right sides of the diagnostics (Equation 1).

Design of experiments for best use of uncertainty estimates of AOD

First part of the work was mostly on explore the CCI observations for dust assimilation, and a proof on the added value of this information for dust forecasts. For this second part of the work, we will focus on the study of the observational uncertainties for the DA system, aiming to make the best use of the uncertainty estimates that CCI data provides in the context of data assimilation.

Before showing the diagnostics for our study case, we announce that the experiments done for this section differ from those of the previous section, even for the same prescription of the observational errors. This has two main causes.

The first is an upgrade of the HPC machine at BSC, from MareNostrum4 to MareNostrum5. Although this should not have a strong impact, there is always the risk of small divergences in the model simulations and DA experiments for research experiments (change of libraries and compilers versions, flags, architecture, etc.).

CMUG CCI+ Deliverable

Reference: Final report WP5.5: Cloud and Aerosol Analysis Study
Due date: August 2024
Submission date: September 2024
Version: 0.4



A second difference with the previous runs is on the dust emission calibration factor. MONARCH allows to calibrate (globally) the dust emissions by a multiplicative factor, that might depend on the input dataset chosen for the experiments, or the model resolution. For the DOMOS experiments, as well as for the first experiments with SLSTR, the calibration was done to approximately unbiased a yearly run of MONARCH over the globe, by comparing MONARCH DOD with filtered AERONET AOD for dusty scenes. This would mimic an operational configuration of global dust forecasts, as the one performed for MONARCH for the ICAP ensemble (<https://aero.und.edu/atmos/icap/index.html>). Therefore, it could be expected that MONARCH underestimate the DOD of the extreme dust event of June. Despite this bias in DOD, the assimilation experiments still show improvements in correlation and errors when SLSTR is assimilated.

The new experiments were prepared to explore the uncertainty description on the assimilation system. Diagnostics of error matrices in the observation space are, in practice, sensitive to biases of the prior. Therefore, the dust emission multiplicative calibration factor was doubled, in accordance with the simple comparison between DOD from MONARCH and the observed dust event DOD. Although still underestimating the dust event, DOD from MONARCH of this second round of experiments perform noticeably better than the first set of experiments.

Estimate of R inflation factor

The diagnostics in the observation space (Equation 1) were computed for the dust event. We use only the diagonal elements of the matrices, and then we compute the ratio of the left to the right hand side of the diagnostics equations, root squared. Binned counts of these ratios are shown in Figure 6. We present the values by value of assimilated AOD from SLSTR (x-axis), and three plots over the domain: all the north Atlantic domain on the left, land of this domain on the middle column and the oceanic part of the domain on the right column. The average ratio is shown in the continuous black line, while the dashed lines indicated the 10, 50 and 90 percentiles of the ratio distribution, grouped by AOD. The continuous green line is the square root of the ratio between the left and right sides of the diagnostic equations. The five correspond to the four diagnostics from Desroziers et al. (2005), in rows 2 to 5, plus a simple ratio of observations to modelled optical depth values, to diagnose biases over the dust plume in the first row.

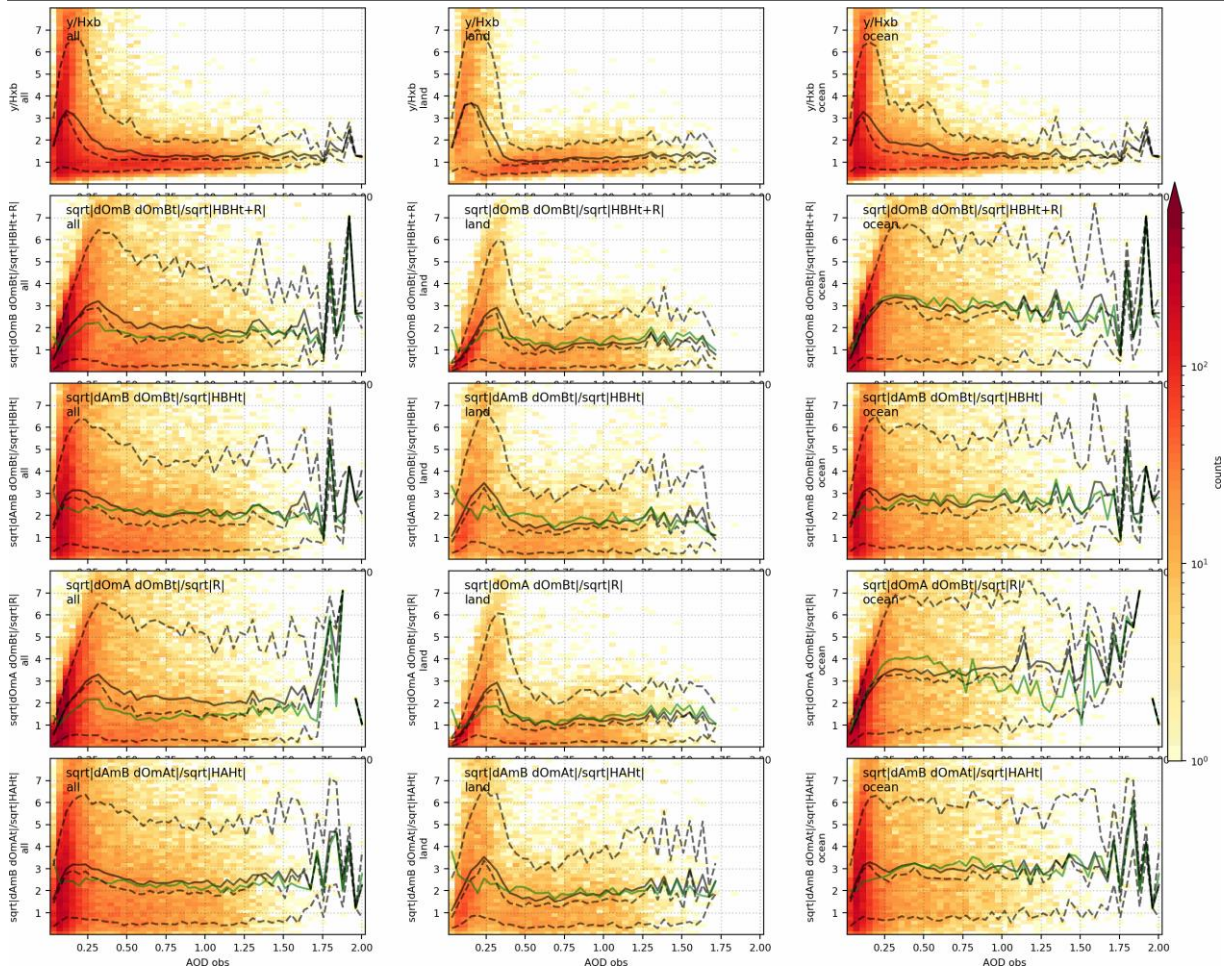


Figure 6: Diagnostics for the experiment that assimilates SLSTR with pixel-wise uncertainties.

The green lines of Figure 6 should be 1 for the ideal case, and it would imply that the trace of the matrices from both sides of the diagnostics equations are equal. There is clear difference between land (middle column) and ocean (right column) panels. Larger values of the ratios over ocean indicates that the **B** and **R** error covariance matrices might be underestimated in the experiments. In the LETKF, the **B** matrix is given by the spread of the ensemble. We have generated the ensemble by using a meteorological ensemble, on top of perturbation over the emissions. Given the positivity constraint on the emissions, the spread of the ensemble cannot be arbitrarily inflated without creating a positive bias. Therefore, we have produced as much spread as possible with this ensemble construction and we acknowledge that **B** might be underestimated in our experiments.

For large AOD over ocean (AOD>0.4), where the dust plume is the predominant aerosol over ocean, the median and mean lines of the diagnostics suggest that the square root of the diagonal elements of the matrices should be inflated by a factor 2 (**B**, 3rd row) or 3 (**R** and **HBH^T + R**, rows 2 and 3). Consequently, we have defined three sensitivity tests, with inflation factors of 2, 3 and 4 over the input observational uncertainties, only over ocean:

- FR : control run without assimilation



- LIN UNC : experiment with linear model for AOD assimilated uncertainties.
- PIX_UNC1: experiment with pixel-level uncertainties for AOD without inflation of uncertainties.
- PIX_UNC2: experiment with pixel-level uncertainties for AOD with double uncertainty over ocean.
- PIX_UNC3: experiment with pixel-level uncertainties for AOD with three times the uncertainty over ocean.
- PIX_UNC4: experiment with pixel-level uncertainties for AOD with four times the uncertainty over ocean.

Results of the sensitivity experiments

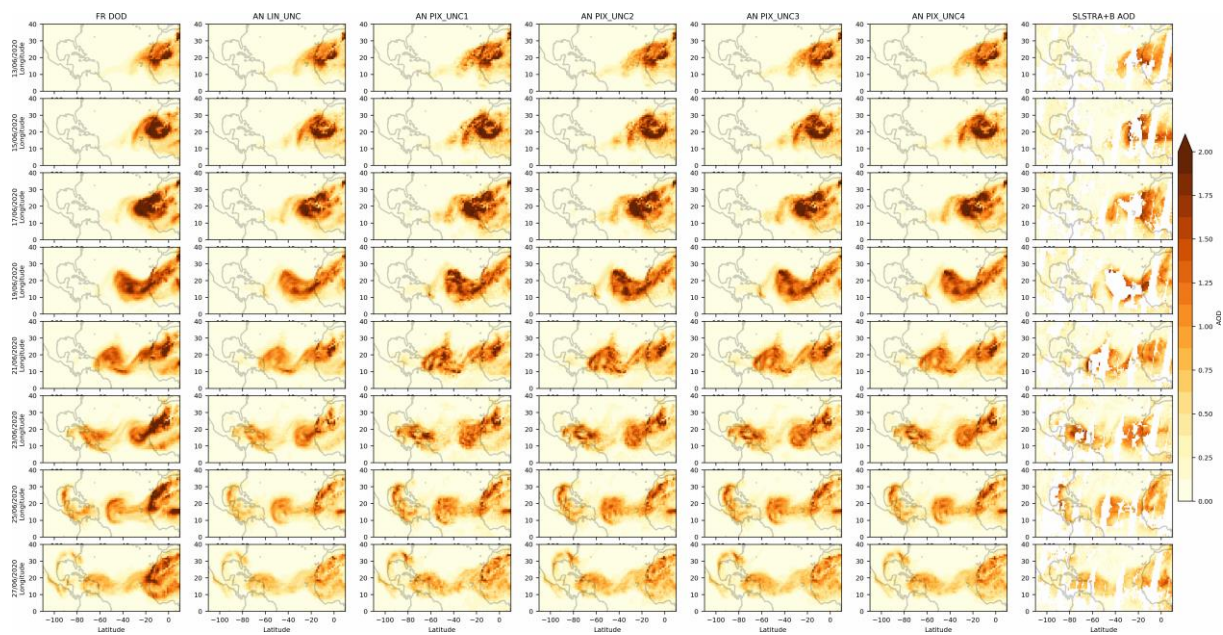


Figure 7: Model and satellite retrievals aerosol information from 18UTC June 13 (top row) to 18UTC June 27 (bottom row) in two-day time steps. Columns: model control run (FR_DOD), analysis of the linear uncertainty experiment (AN LIN UNC), analysis of the pixel-level uncertainty with inflation over ocean equal one (AN PIX_UNC1), two (AN PIX_UNC2), three (AN PIX_UNC3) and four (AN PIX_UNC4), and SLSTR AOD.

Figure 7 shows the analyses DOD from the sensitivity experiments for the dust event. Control run is shown in the left column, while SLSTR AOD observations are shown in the last column. Second column shows the analyses where the observational error was assumed with a linear uncertainty of the AOD observations, while columns 3 to 6 show the sensitivity test with different inflation factors for the pixel level uncertainties over ocean. Compared with the initial results on the assimilation (D2.0e), the control run and the analyses are less biased. Qualitatively, the analyses that make use of the pixel-level uncertainty show more small scale

CMUG CCI+ Deliverable

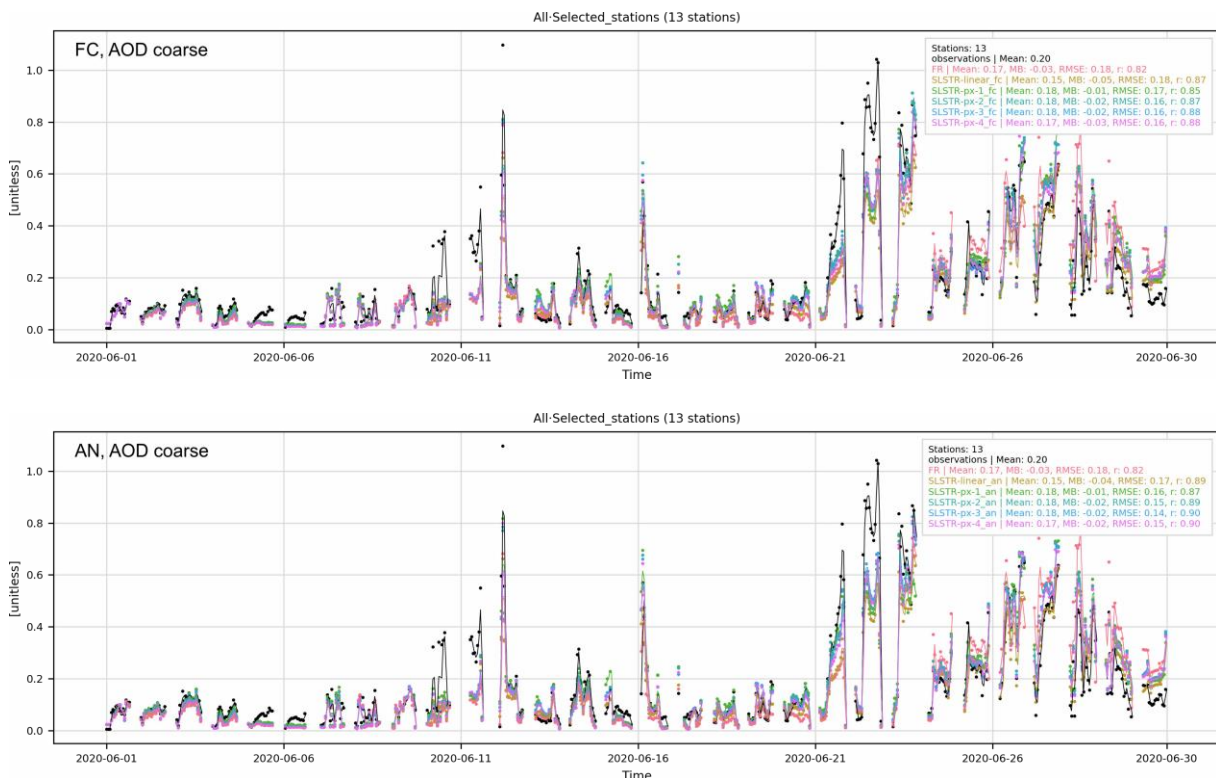
Reference: Final report WP5.5: Cloud and Aerosol Analysis Study
Due date: August 2024
Submission date: September 2024
Version: 0.4



features that the control run or the analysis with linear uncertainties. The likely noise pattern of the pixel-level uncertainty assimilation without inflation (AN_PIX_UNC1) is smoothed progressively as the inflation is larger. Still, qualitative differences can be appreciated between the LIN_UNC and all PIX_UNC experiments.

We have collocated the simulations with AERONET measurements. For dust filtering of AERONET AOD, we will show two approaches. The first one (used for example in DOMOS project and D2.0e) is to compare coarse AOD with model coarse DOD over sites with predominance of dust. A second approach is to filter AERONET AOD by measurements with low Angstrom exponent over dusty sites (e.g. Klose et al 2021, Escribano et al. 2022). For each experiment, we show two model simulations: analyses and forecasts. Analyses are the result of the data assimilation procedure, while the forecasts are the average of the model ensemble daily forecast, that is, the forecasts initialised by analyses at 0 UTC that serves as prior for the next 24-hours assimilation cycle. We use the same AERONET sites of the D2.0e verification (Figure 3).

Figure 8 shows the time series of the AERONET comparison with forecasts and analyses for all the (spatially averaged) stations depicted in Figure 3, for analyses and forecast simulations, and for coarse and total AOD. All the assimilating experiments show a better comparison than the control run with respect to AERONET observations with, as expected, better scores reached by the analyses experiments over the forecasts. Although the model DOD is in average underestimated, overestimations are more important in experiments with lower inflations of uncertainties.



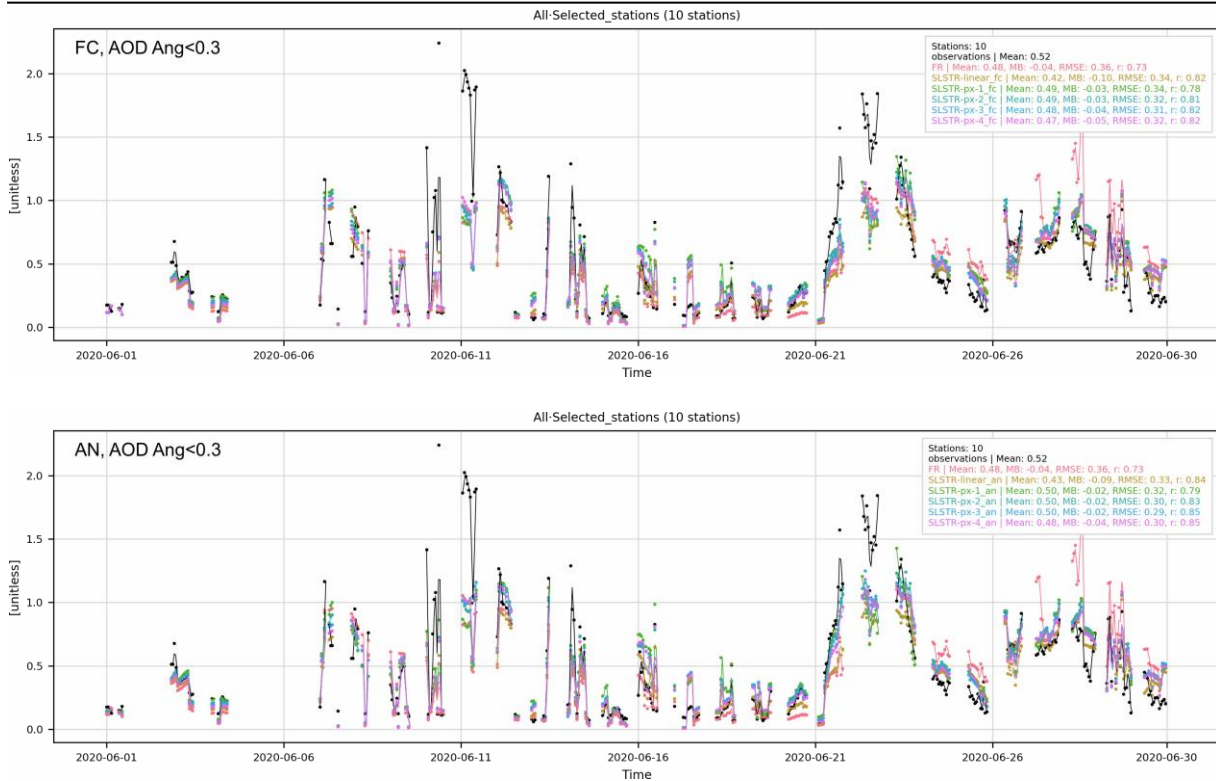


Figure 8: Time series of averaged model DOD and AERONET AOD. Rows: collocated MONARCH coarse DOD and AERONET DOD for the forecasts run; collocated MONARCH coarse DOD and AERONET DOD for the analyses; collocated MONARCH DOD and AERONET DOD (Angstrom exponent <math>< 0.3</math>) for the forecasts run; collocated MONARCH DOD and AERONET DOD (Angstrom exponent <math>< 0.3</math>) for the analyses.

Time series of Figure 8 do not allow to visually track the transport of the dust. Figure 9 shows the model forecasts for three selected stations, sorted from east to west in concordance with the arrival of the dust plume over the Caribbean. While the control run underestimates the first peak of AOD in these three sites, the analyses are low biased in the two eastern sites. Bias, RMSE and correlation coefficients are better in experiments that assimilate pixel-level uncertainty than the experiment with linear uncertainty assumption (which is also better than the control run). Experiments with smaller inflation of AOD uncertainty over ocean show, in average, larger values of AOD than those with larger inflation factors, implying better bias scores. The correlation and RMSE reach best values with inflation equal 2 for Ragged Point, equal 3 in La Parguera and equal 4 in NEON OSBS, although the differences between values of the scores of different runs is small. Qualitatively, the experiments with pixel-level uncertainty are able to enhance or suppress parts of the plume spatial structure (Figure 7) and the arrival time of the dust plume over the Caribbean: the AOD from the SLSTR-px experiments peaks 6 hour earlier over La Parguera and Ragged Point; which explain the differences of the experiment AOD on June 21th at that site.

CMUG CCI+ Deliverable

Reference: Final report WP5.5: Cloud and Aerosol Analysis Study
 Due date: August 2024
 Submission date: September 2024
 Version: 0.4

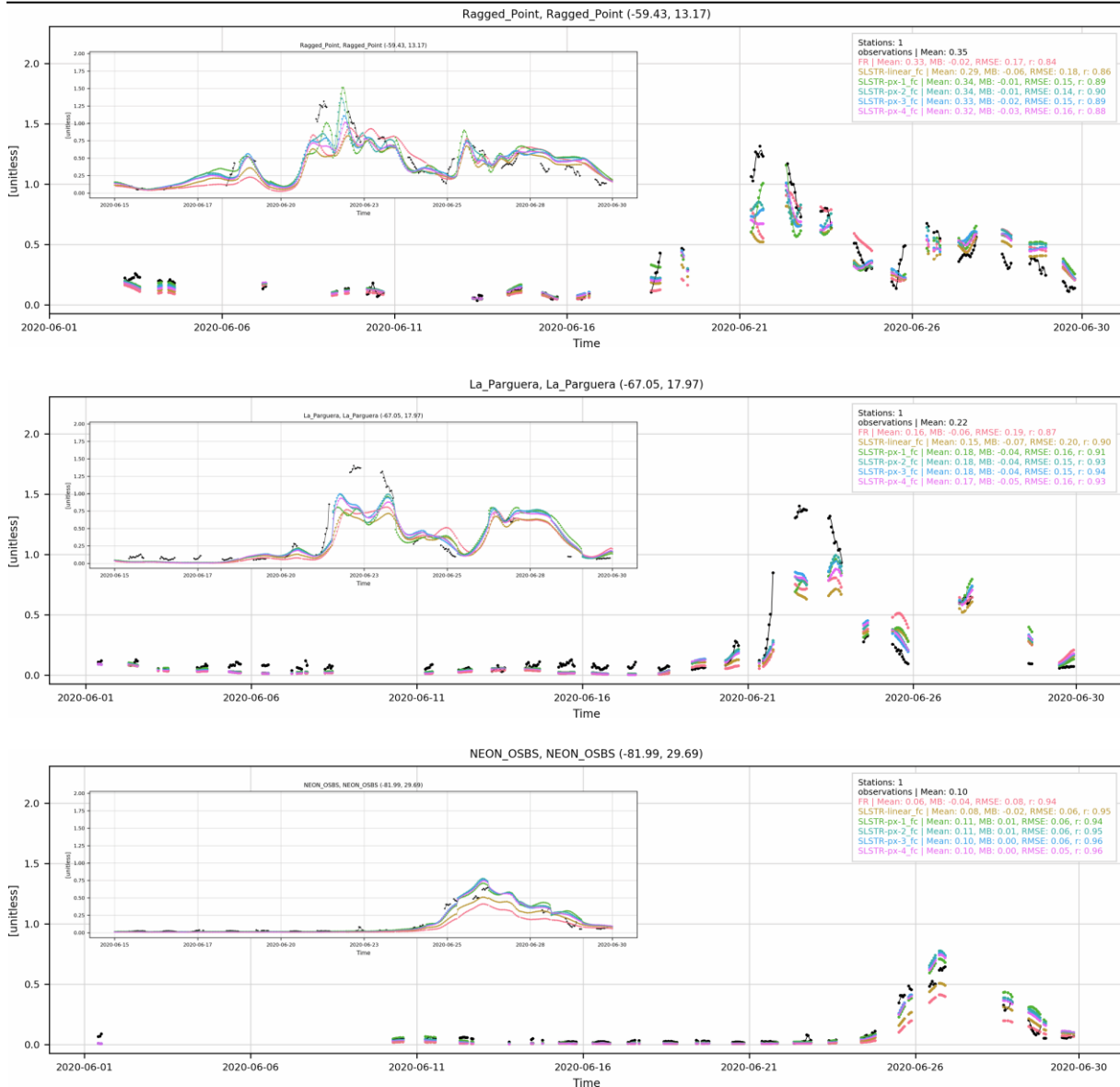


Figure 9: Time-series of coarse AOD AERONET retrievals and model forecasts for three AERONET sites: Ragged Point, La Parguera and NEON OSBS. Colour code is shown in the panel legends, with FR the control run and SLSTR-* the five experiments with different assumptions on the observational uncertainty. Model time series without temporal collocation with AERONET for the last 15 days are shown in the upper right corner of each panel.

Similar plots for the analyses are presented in Figure 10. Here, the overall scores are better than the forecasts, and the pixel-level uncertainty experiments show also better scores than the linear assumption of the uncertainty assimilation experiment. Larger inflation degrades the scores over Ragged Point, but not over La Parguera and NEON OSBS.

CMUG CCI+ Deliverable

Reference: Final report WP5.5: Cloud and Aerosol Analysis Study

Due date: August 2024

Submission date: September 2024

Version: 0.4

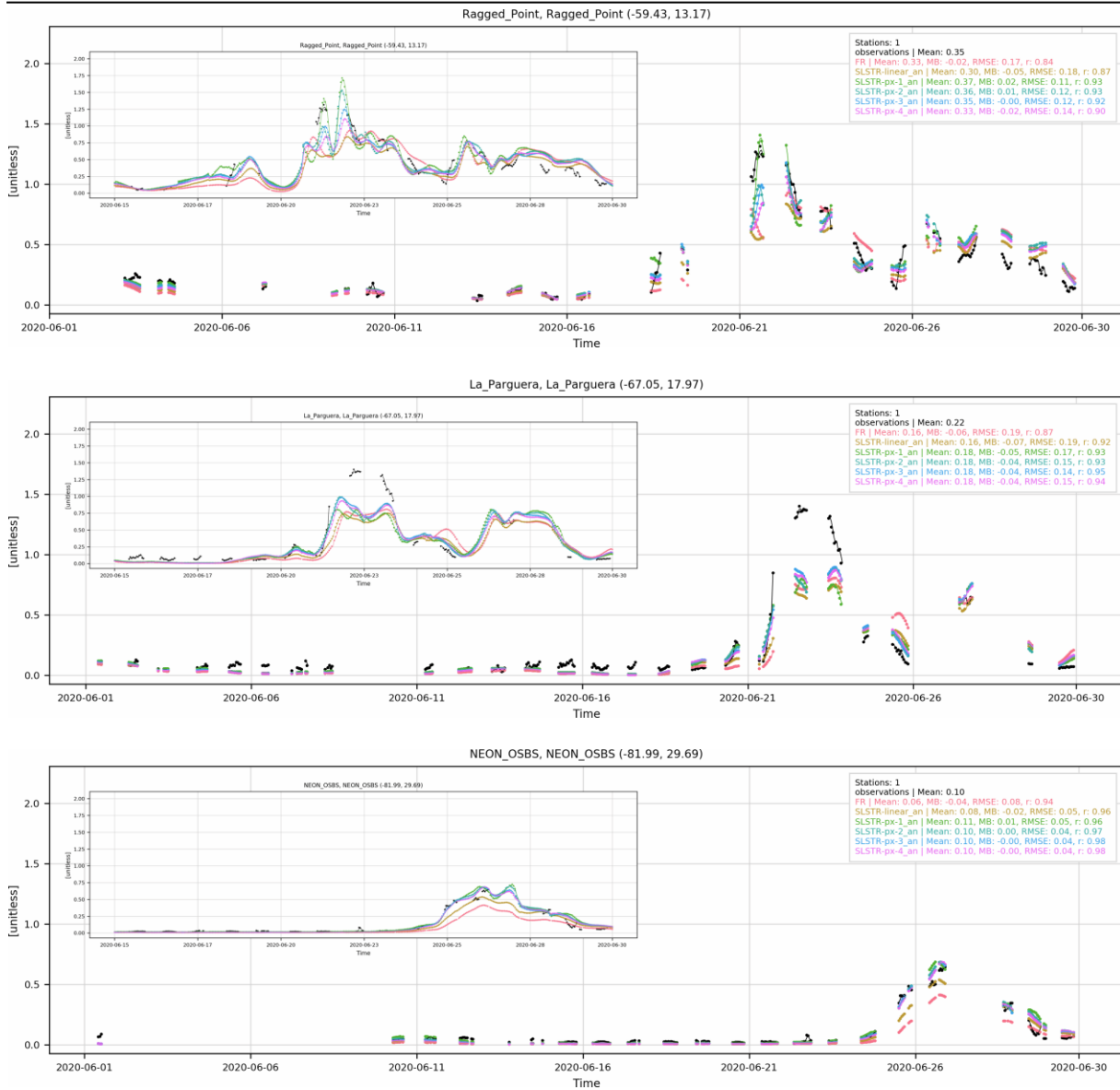


Figure 10: Same as Figure 9 but for the model analyses.

We present a summary of scores in four tables, for coarse AOD and filtered AOD by Angstrom exponent, and for forecasts and analyses experiments. Table 2 show the scores of the forecasts with respect to AERONET coarse AOD. All experiments with pixel-level uncertainty have better scores than the linear uncertainty experiment (and the control). Larger inflation of oceanic uncertainties increases the bias scores but improves the error scores, as well as the correlation coefficient.

CMUG CCI+ Deliverable

Reference: Final report WP5.5: Cloud and Aerosol Analysis Study
 Due date: August 2024
 Submission date: September 2024
 Version: 0.4



FC	Mean	p50	Std.	MB	NMB	MFB (%)	MAE	NME	MFE (%)	RMSE	r
Obs.	0.20	0.07	0.31	----	-----	-----	----	-----	-----	----	----
Coarse AOD											
FR	0.17	0.04	0.25	0.03	13.23	-30.93	0.09	46.94	69.75	0.18	0.82
SLSTR-linear	0.15	0.05	0.20	0.05	23.14	-26.78	0.08	41.42	62.90	0.18	0.87
SLSTR-px1	0.18	0.06	0.24	0.01	-7.34	-6.30	0.08	42.06	57.63	0.17	0.85
SLSTR-px2	0.18	0.06	0.24	0.02	-8.97	-13.00	0.08	39.45	59.81	0.16	0.87
SLSTR-px3	0.18	0.05	0.24	0.02	10.70	-16.65	0.08	39.31	61.55	0.16	0.88
SLSTR-px4	0.17	0.05	0.23	0.03	12.91	-19.49	0.08	39.72	62.49	0.16	0.88

Table 2: Scores for the forecasts compared with AERONET coarse AOD. Columns show the AOD computed scores: Mean (Mean), median (p50), standard deviation (Std.), mean bias (MB), normalised mean bias (NMB), mean fractional bias (MFB), mean absolute bias (MAE), normalised mean error (NME), mean fractional error (MFE), root mean squared error (RMSE) and Pearson correlation coefficient (r). Rows indicate the AERONET observations, the control run MONARCH simulation (FR) and the five MONARCH experiments assimilating SLSTR: with linear uncertainties (SLSTR-linear), and with inflation of uncertainties over ocean, for factors 1 to 4 (SLSTR-px1 to SLSTR-px4).

Same scores against coarse AOD but for the analyses are shown in Table 3. Similar to the forecasts, low inflation experiment shows better scores in bias, but not in error. A small difference with the forecasts is that best scores are reached for inflation equal 3 instead of inflation equal 4 of the forecasts. Nonetheless, the improvements in the scores are relatively small.

AN	Mean	p50	Std.	MB	NMB	MFB (%)	MAE	NME	MFE (%)	RMSE	r
Obs.	0.20	0.07	0.31	----	-----	-----	----	-----	-----	----	----
Coarse AOD											
FR	0.17	0.04	0.25	0.03	13.23	-30.93	0.09	46.94	69.75	0.18	0.82
SLSTR-linear	0.15	0.05	0.21	0.04	21.72	-24.80	0.08	38.71	60.63	0.17	0.89
SLSTR-px1	0.18	0.07	0.24	0.01	-6.79	-3.37	0.08	38.57	55.22	0.16	0.87
SLSTR-px2	0.18	0.06	0.24	0.02	-7.83	-10.69	0.07	36.40	57.73	0.15	0.89

CMUG CCI+ Deliverable

Reference: Final report WP5.5: Cloud and Aerosol Analysis Study
 Due date: August 2024
 Submission date: September 2024
 Version: 0.4



SLSTR-px3	0.18	0.06	0.24	0.02	-8.70	-14.40	0.07	35.46	59.58	0.14	0.90
SLSTR-px4	0.17	0.05	0.24	0.02	11.30	-17.71	0.07	36.15	60.47	0.15	0.90

Table 3: Scores for the analyses compared with AERONET coarse AOD. Columns and rows as in Table 2.

Score for the forecast DOD with respect to AERONET AOD filtered by Angstrom exponent is shown in Table 4, while Table 5 show the scores for the analyses. In both cases the bias and the normalised bias show better scores for the pixel-level uncertainty experiment without inflation, while mean fractional bias show better scores when the inflation is large. Correlation and error scores are similar for inflations factors of 2, 3 and 4, while slightly worse when no inflation is applied to the AOD uncertainty over ocean.

FC	Mean	p50	Std.	MB	NMB	MFB (%)	MAE	NME	MFE (%)	RMSE	r
AOD Ang. < 0.3											
Obs.	0.52	0.32	0.53	----	----	----	----	----	----	----	----
FR	0.48	0.42	0.39	0.04	-8.35	11.03	0.22	42.16	47.24	0.36	0.73
SLSTR-linear	0.42	0.38	0.30	0.10	19.13	11.47	0.19	36.17	40.25	0.34	0.82
SLSTR-px1	0.49	0.44	0.35	0.03	-5.07	5.67	0.20	38.72	41.28	0.34	0.78
SLSTR-px2	0.49	0.42	0.35	0.03	-5.54	4.07	0.19	35.98	40.24	0.32	0.81
SLSTR-px3	0.49	0.40	0.35	0.04	-7.36	1.73	0.18	35.54	40.24	0.31	0.82
SLSTR-px4	0.49	0.40	0.34	0.05	-9.06	-0.48	0.18	35.53	40.24	0.32	0.82

Table 4: Scores for the forecasts compared with AERONET AOD with Angstrom exponent less than 0.3. Columns and rows as in Table 2.

AN	Mean	p50	Std.	MB	NMB	MFB (%)	MAE	NME	MFE (%)	RMSE	r
AOD Ang. < 0.3											
Obs.	0.52	0.32	0.53	----	----	----	----	----	----	----	----
FR	0.48	0.42	0.39	0.04	-8.35	11.03	0.22	42.16	47.24	0.36	0.73
SLSTR-linear	0.43	0.37	0.31	0.09	17.91	-9.73	0.18	33.93	37.91	0.33	0.84
SLSTR-px1	0.50	0.44	0.37	0.02	-3.39	7.31	0.18	34.97	38.32	0.32	0.79

CMUG CCI+ Deliverable

Reference: Final report WP5.5: Cloud and Aerosol Analysis Study
Due date: August 2024
Submission date: September 2024
Version: 0.4



SLSTR- px2	0.50	0.43	0.37	-	-3.41	5.84	0.17	33.36	37.99	0.30	0.83
SLSTR- px3	0.50	0.42	0.36	-	-4.50	4.15	0.17	32.02	38.21	0.29	0.85
SLSTR- px4	0.48	0.41	0.35	-	-7.01	1.08	0.17	32.52	37.96	0.30	0.85

Table 5: Scores for the analyses compared with AERONET AOD with Angstrom exponent less than 0.3. Columns and rows as in Table 2.

In summary, all assimilation experiments outperform the control run when they are compared to both AERONET AOD datasets. Between assimilation experiments, those that make use of the pixel-level uncertainty can show better scores than the experiment that use a model of linear uncertainties. For coarse AOD comparison, larger uncertainty inflation improves the error scores and the correlation coefficient but degrades the bias scores. For AOD filtered by Angstrom exponent, the degradation in the mean bias and the improvement in the correlation coefficient are clear, and the improvements in error scores are very small (but positive).

Diagnostics for the experiment with inflation of uncertainties over ocean

After performing the experiments, we compute the same diagnostics of Figure 6, but for the experiment with inflation equal 3 in Figure 11. In an ideal case, the ratio shown in this Figure should be close to 1. In our case, comparing the plots of the right column (i.e., over ocean) with those of Figure 6 there is a decrease in the mean and median values, pointing to smaller differences between the innovations or increments and the error matrices in the observational space. The spread of these values is also decreased. For $AOD < 0.4$, the diagnostics in Figure 11 show a noticeable decrease of the ratios. For $AOD > 0.4$ over ocean (which would correspond to the dust plume), the mean and median lines of diagnostic ratios of the **B** matrix panel (3rd row) are slightly changed. This is expected because, despite changes in \mathbf{d}_b^a , the ensemble construction and prior spread remain practically unchanged between experiments. In Figure 11, the mean and media ratios of the **R** diagnostic panel (4th row) and the $\mathbf{HBH}^T + \mathbf{R}$ show smaller values those of Figure 6, but still they do not reach unity. This is also the case for the diagnostic of the other two sensitivity experiments with inflation equal 2 and inflation equal 4, not shown here. We hypothesis that is possible that biases and the plume location mismatch of the system, consequence of a pixel by pixel comparison, hamper the optimal use of these diagnostics equations.

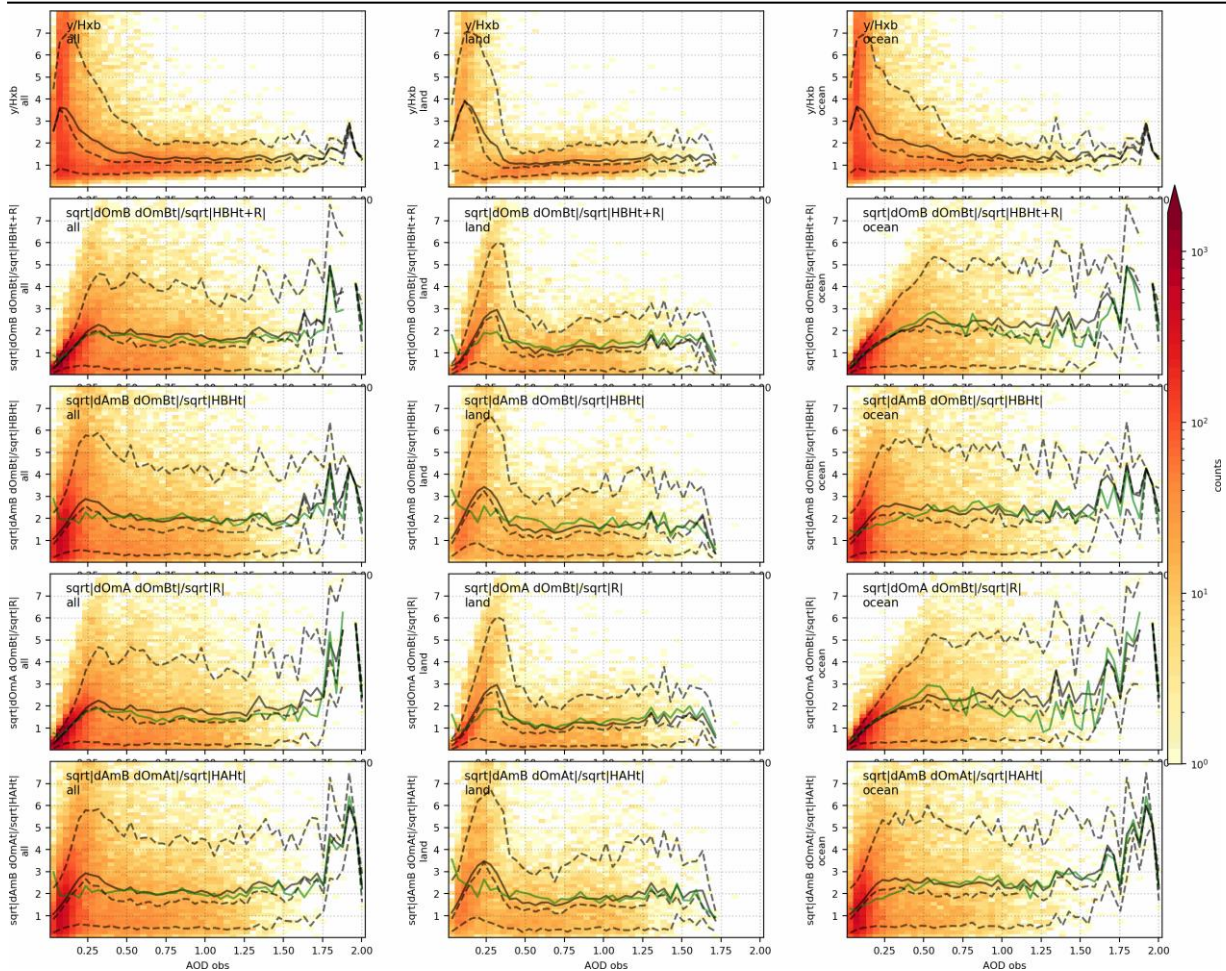


Figure 11: Same as Figure 6 but for inflation equal 3 for the uncertainties over ocean.

Summary and recommendations

We have tested the assimilation of SLSTR SU v1.14 products in the BSC MONARCH-LETKF dust data assimilation system for the Godzilla extreme dust event of June 2020. Visual inspection shows an underestimation of the Dust AOD product of SLSTR-SU v1.14. Coarse AOD, computed by AOD minus fine AOD, is also underestimating the aerosol optical load. Assimilation experiments using SLSTR SU v1.14 AOD were performed. For a model calibration agnostic to the extreme dust event of June 2020, the control run underestimates the dust plume. Assimilation experiments using SLSTR AOD show improvements in skill scores with respect to the control when ground-based AOD is used as reference. The skills are comparable to those assimilation experiments of the DOMOS project (with VIIRS and LIVAS). SLSTR assimilation that uses the pixel-level uncertainty of the SU product show better quantitative verification metrics with respect to AERONET than the experiment that assumes a linear model for the uncertainty. A possible overfitting of the observations is identified in the AOD analyses fields, which is possibly due the effect of an underestimation of the SLSTR AOD uncertainty over ocean in the data assimilation procedure.

CMUG CCI+ Deliverable

Reference: Final report WP5.5: Cloud and Aerosol Analysis Study
Due date: August 2024
Submission date: September 2024
Version: 0.4



We have produced a new set of experiments to test and estimate better the AOD uncertainties over ocean by means of inflating the pixel-wise provided uncertainties. For this, we have re-calibrated the experiments to produce a less biased prior, targeted to this extreme dust event. All in all, we conclude that inflation of factor 2 to 3 of the uncertainty associated to the assimilated observation can provide:

- Better skill scores in comparison to the linear case or to the case without observational uncertainty inflation
- Less noise in spatial fields of analyses
- More consistent error diagnostics in the observational space

It is important to stress that the inflation of \mathbf{R} implemented here has no one-to-one correspondence to the SLSTR observations uncertainty of AOD provided in the dataset. Following the terminology of Janjić et al. (2017), the \mathbf{R} error covariance matrix accounts for the covariance of the observational error, which is the assimilated observational value minus the (unknown) true value. This observational error consists of the representation error and the measurement error. The uncertainty reported in the SLSTR product would be equivalent to the measurement error in the terminology of Janjić et al. (2017). The representation error includes the observation operator error, the pre-processing error and the errors due to unresolved scales and processes. Part of the inflation used here might account for errors in the observation operator (e.g. dust optics), errors in the aggregation and filtering of observations, the coarser model spatial and temporal resolution, or the assumption that most of the observed AOD in the plume corresponds to DOD.

Recommendations to CCI data providers

We have shown that SLSTR AOD can be ingested in an operational-like data assimilation workflow to produce dust forecasting and produce better skills. We might largely benefit from an improved version of visible dust AOD from CCI SLSTR retrievals, with their corresponding uncertainty estimates. Experiments with SLSTR pixel-level uncertainties improve the accuracy of the data assimilation analyses and products. Dust AOD with pixel-level uncertainties should provide even better results. We also indicate that the experiments perform better when an inflation factor is applied over the oceanic uncertainties. We suggest that these uncertainties are underestimated in the data assimilation system, and this underestimation might be due underestimation of the retrieval uncertainty, but also might be inherent to the data assimilation system, as part of the representation error.

CMUG CCI+ Deliverable

Reference: Final report WP5.5: Cloud and Aerosol Analysis Study
Due date: August 2024
Submission date: September 2024
Version: 0.4



3. WP5.5.2 Cloud/Aerosol analysis with the ECMWF system

Lead partner: ECMWF

Authors: Kirsti Salonen and Angela Benedetti

Aim

The work package aims to implement and test Climate Change Initiative (CCI) products for aerosol optical depth (AOD) and cloud optical depth (COD) for active assimilation from the Sea and Land Surface Temperature Radiometer (SLSTR) onboard the Sentinel 3 satellites in the European Centre for Medium Range Forecasts (ECMWF) system. AOD data is provided by the Swansea University, v1.14 (personal communication P. North and K. Pearson) and COD data by Science and Technology Facilities (STFC) and Deutscher Wetter Dienst (DWD). The COD v3.3 dataset is not part of the official CCI data sets, but the same algorithms are being used to cover the test periods June 2020 and September 2021 (personal communication M. Stengel and G. Thomas, 2023).

Summary of the technical preparations

In order to allow active assimilation of the CCI AOD and COD observations, a set of technical preparations has been carried out. Both data sets are provided in netCDF format. The first step is to create Observation Data Base (ODB) files from the observations. ODB is the internal data format used in the ECMWF system. The AOD and COD need their own processing chains which have been developed and implemented offline in python. The ODB files cover the 12-hour data assimilation window used in the ECMWF 4D-Var and include all quality information from the original netCDF files to allow flexible quality control in the assimilation experiments. For COD data the processing includes also re-formatting the 3-dimensional (time, lat, lon) global netCDF files into 1-dimensional as the ODB was not able to handle the original format. Also the COD data is pre-thinned to every 5th observation. This was required to resolve technical problems related to interpolating the model profiles to the observation location. To reduce the COD ODB file size to manageable, only observations over sea have been included. Table 6 and Table 7 summarize the variables included to the ODB files for AOD and COD, respectively.

Table 6: Summary of the variables in the AOD netCDF files and the corresponding variables in the ODB files.

Variable name in the original netCDF file	Variable name in the ECMWF system	Variable value if constant
	reportype	98001
	groupid	99
	obstype	7
	codetype	206
	sensor	180
	distribtype	0
	seqno	0

CMUG CCI+ Deliverable

Reference: Final report WP5.5: Cloud and Aerosol Analysis Study
 Due date: August 2024
 Submission date: September 2024
 Version: 0.4



time	date	using yyyymmdd_from_epoch(time)
time	time	using hhmmss_from_epoch(time)
latitude	lat	
longitude	lon	
AOD550	obsvalue	
	varno	174
	vertco_reference_1	0.00000055
satellite_zenith_at_center	zenith	
relative_azimuth_at_center	azimuth	
sun_zenith_at_center	solar_zenith	
surface_type_number	land_fraction	
pixel_corner_latitude1	lat_fovcorner_1	
pixel_corner_latitude2	lat_fovcorner_2	
pixel_corner_latitude3	lat_fovcorner_3	
pixel_corner_latitude4	lat_fovcorner_4	
pixel_corner_longitude1	lon_fovcorner_1	
pixel_corner_longitude2	lon_fovcorner_2	
pixel_corner_longitude3	lon_fovcorner_3	
pixel_corner_longitude4	lon_fovcorner_4	
surface_type_number	surface_type_indicator	
cloud_fraction	cloud_cover	
pixel_number	scanpos	
AOD550_uncertainty	final_obs_error	
	satellite_identifier	61 Sentinel 3A 65 Sentinel 3B

Table 7: Summary of the variables in the COD netCDF files and the corresponding variables in the ODB files.

Variable name in the original netCDF file	Variable name in the ECMWF system	Variable value if constant
	reportype	98002
	groupid	99
	obstype	7
	codetype	206
	sensor	180
	distribtype	0
	seqno	0
yyyymmdd_from_epoch(time_desc)	date	

CMUG CCI+ Deliverable

Reference: Final report WP5.5: Cloud and Aerosol Analysis Study
Due date: August 2024
Submission date: September 2024
Version: 0.4



hhmss_from_epoch(time_desc)	time	
lat	lat	
lon	lon	
cot_desc	obsvalue	
	varno	175
	vertco_reference_1	0.00000055
satzen_desc	zenith	
relazi_desc	azimuth	
solzen_desc	solar_zenith	
qcflag_desc	quality_retrieval	
illum_desc	surface_type_number	Note, existing ODB variable name used just for testing
cmask_desc	surface_type_indicator	Note, existing ODB variable name used just for testing
cot_desc_unc	final_obs_error	
	satellite_identifier	61 Sentinel 3A 65 Sentinel 3B

Observation operator for AODs

AOD observations from other instruments are used operationally in the ECMWF Copernicus Atmosphere Monitoring Service (CAMS) configuration so the observation operator was ready for the CCI data as well without modifications. In general, an observation operator maps the model counterpart for each observation to the observation location in space and in time. For AOD the observation operator consists of deriving the modelled AOD from the mixing ratio value using the observation operator documented in Benedetti et al. (2009).

Observation operator for CODs

COD data is not used operationally in the ECMWF system, so implementing it has required more technical work than AOD. The ECMWF system has now been updated to allow active assimilation of COD. The observation operator is described in detail in Benedetti et al. (2008). However, it needed some technical updates to be compatible with the current operational framework, the observation operator was tested in the IFS cycle 48R1. IFS documentation is available online at <https://www.ecmwf.int/en/forecasts/documentation-and-support/changes-ecmwf-model/ifs-documentation>.



Designing quality control and observation errors

The AOD and COD observation quality has been evaluated in the ECMWF system with passive monitoring experiments. Passive monitoring means that the model counterpart for the observation is calculated with the corresponding observation operator but the observation has no impact in the analysis or resulting forecasts, i.e. it is passive. The monitoring experiments are a powerful way to design quality control for the new observations as well as to design realistic observation errors to be used in the active assimilation. The data periods cover June 2020 and September 2021.

Figure 12 shows the observation minus model background (OmB) bias (left panel) and standard deviation (right panel) for AOD observations in June 2020 over sea. In general, the data quality over sea is good, the bias is close to zero except in the tropics 75W – 80W which is related to desert dust. The bias is season dependent as can be seen in Figure 13 left panel where the bias is shown for September 2021. The OmB standard deviation, indicating the magnitude of random errors is also relatively homogeneous over sea except the regions where the desert dust related bias is visible.

Figure 14 (June 2020) and Figure 15 (September 2021) show similar statistics but over land. In general, the statistics over land are more heterogeneous than over sea. The biases are season and location dependent and also the random errors are significantly higher in magnitude than over sea. Thus, at the first stage it is concluded that the active assimilation experiments should focus on data over sea only.

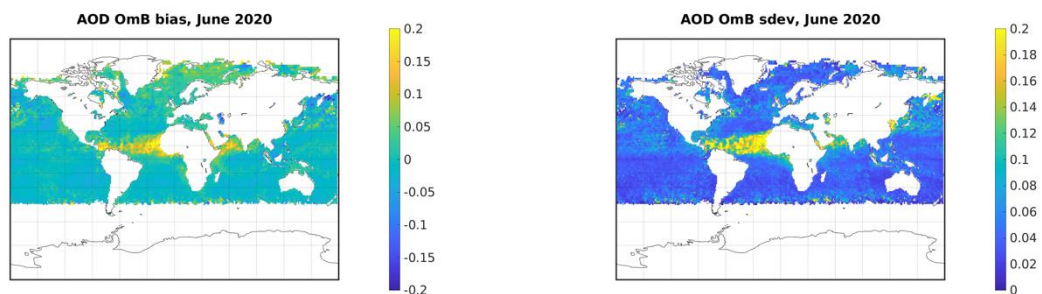


Figure 12: Observation minus model background bias (left panel) and standard deviation (right panel) for June 2020.

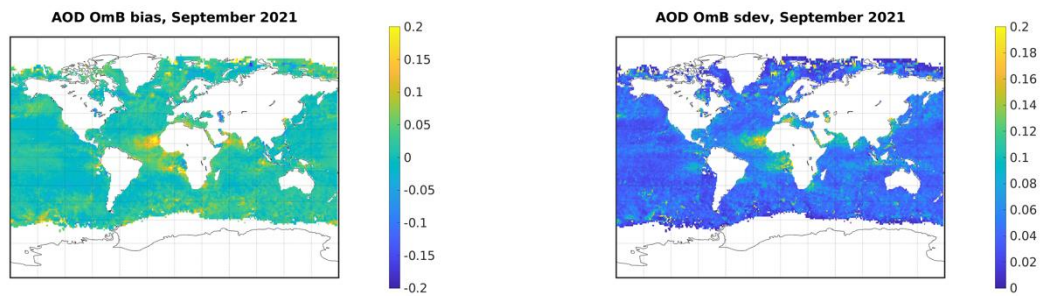


Figure 13: Similar to Figure 12 but for September 2021.

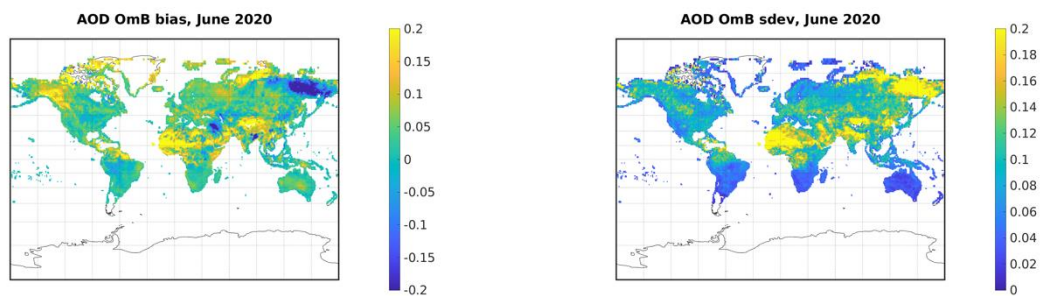


Figure 14: Similar to Figure 12 but over land.

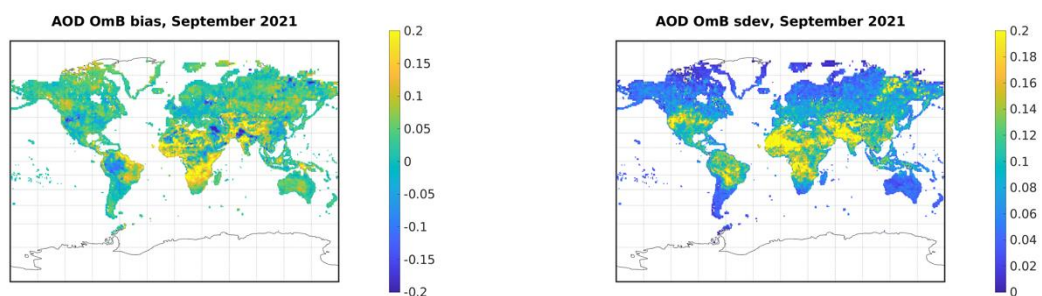


Figure 15: Similar to Figure 13 but over land.

The AOD observations are provided with uncertainty estimates. By nature, this is a scene dependent estimate of the observation error. Another estimate for the observation error is provided by the OmB standard deviation statistics. These two error estimates are compared in Figure 16. The OmB standard deviation includes naturally also the error component of the model background. However, it is often a realistic first estimate of the magnitude of the error as there are error sources which are not explicitly taken into account in the uncertainty estimate provided, such as observation error correlations, representativeness errors or errors in the



observation operator. Both of the study periods indicate that over sea the OmB standard deviation is roughly 2 times larger than the uncertainty estimate provided with AODs.

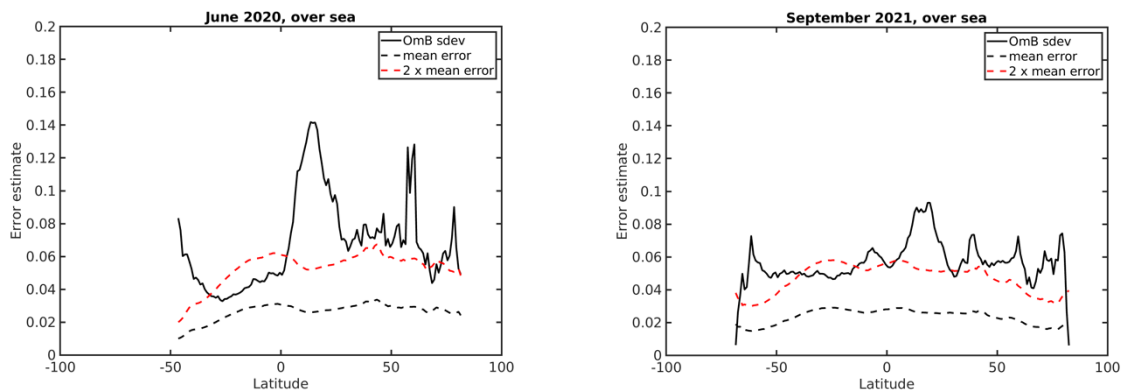


Figure 16: Zonal plot of the OmB standard deviation (black solid line), mean uncertainty estimate (black dashed line) and 2 times mean uncertainty estimate (red dashed line) for June 2020 (left panel) and September 2021 (right panel).

The quality and characteristics of the COD observations have been assessed with passive monitoring experiments covering June 2020 and September 2021. Figure 17 shows the OmB mean difference and standard deviation for September 2021 for all COD observations over sea. Positive mean differences, i.e. observed COD higher than model background, are seen over regions where there is typically persistent marine stratus. Negative mean difference on the other hand is seen especially over the inter-tropical convergence zone where also increased magnitude of the OmB standard deviation is evident. Same features are also seen for the June 2020 period (not shown). Passive monitoring of reflectance observations from the Ocean and Land Colour (OLCI) instrument indicate very similar mean difference features (personal communication S. Quesada Ruiz) which suggests that the features seen are potentially related to model deficiencies over those areas.

The COD observations are provided with quality flags and to screen highest quality observations for active assimilation, it has been decided to accept only COD observations where none of the quality flags is raised. This is roughly 90% of all data. However, using the quality flags alone for quality screening has only a minor impact to the OmB statistics. As an additional quality screening it has been decided to limit the COD values, both observed and model counterparts, to 80 to exclude unrealistic and highly saturated cases. Figure 18 is showing the OmB statistics after the quality screening. The impact on OmB bias is rather small but the OmB standard deviation, illustrating the magnitude of random errors, is decreased quite significantly.

Left panel of Figure 19 shows the distribution of the COD values for the quality screened data, black bars are indicating the observed values and the grey bars the model counterparts. Observed COD has higher number of cases with COD less than 6 while the distribution of the model background COD is flatter. The right panel of Figure 19 shows the OmB departure distribution. It is slightly skewed to the negative side, i.e. the globally the model background values are on average higher in magnitude than the observed values. Locations of the strongest negative biased areas are over the Tropics as seen in Figure 17 and Figure 18. The monitoring statistics indicate that the assimilation would likely benefit from developing and implementing a bias correction scheme. However, within the framework of this project that was not feasible, and the first assimilation trials have been performed without applying any bias correction.

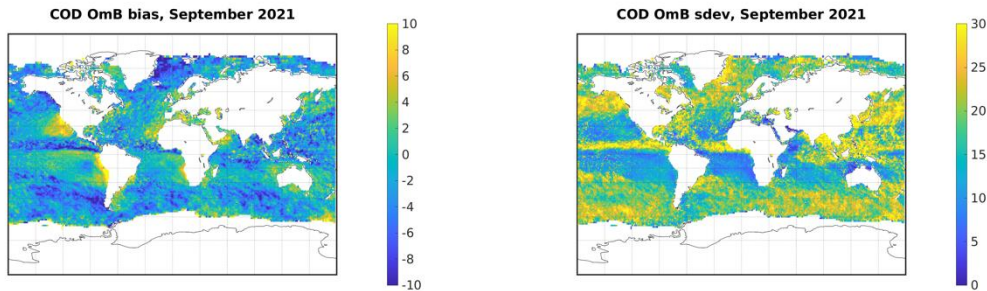


Figure 17: Observation minus model background bias (left panel) and standard deviation (right panel) for September 2021, all observations are included into the comparison.

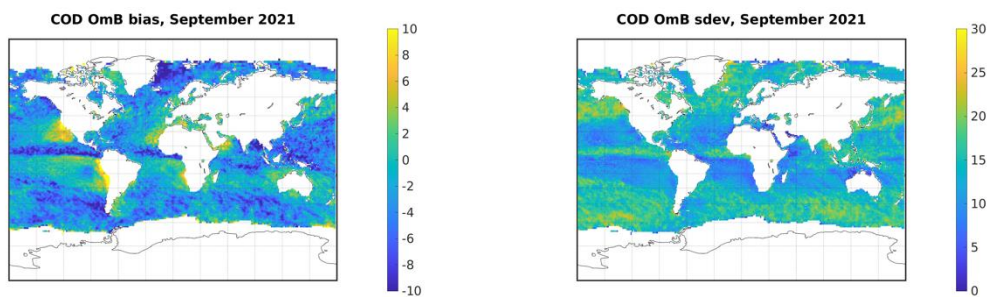


Figure 18: Similar to Figure 17 but for quality screened data.

In order to estimate the magnitude of observation errors to be used in the assimilation experiments, the uncertainty estimates provided with the data have been compared to the OmB standard deviation statistics. The comparison for September 2021 is shown in Figure 20. The results are similar for June 2020 and thus not shown. The OmB standard deviation is 8-9 times the magnitude of the uncertainty estimates for all the data (black lines) and around 6 times larger for the screened data (grey lines). The magnitude of the averaged uncertainty estimates does not change notably whether the quality screening is applied to the data but the magnitude of the OmB standard deviation, which is a measure for the magnitude of the random errors, decreases significantly. The magnitude of the OmB standard deviation is typically a good first guess for the magnitude of the observation errors as discussed earlier related to the AOD observation errors. Thus, in the first assimilation experiments $0.75 \times$ observed COD has been used as observation error. This matches on average very well the magnitude of the average OmB standard deviation as shown in the right panel of Figure 20.

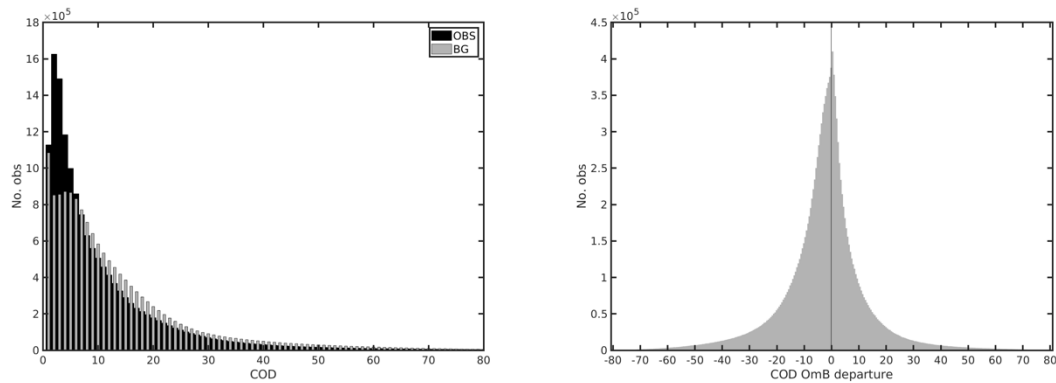


Figure 19: Distribution of observed (black) and model background COD values (grey) (left panel) and distribution of the OmB values (right panel) for the quality screened data. Considered period is September 2021.

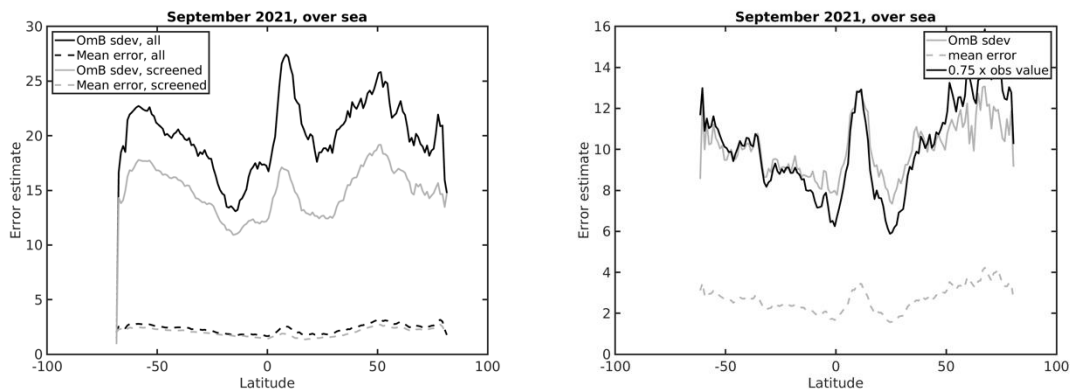


Figure 20: The left panel shows zonal average of the mean uncertainty provided with the COD observations (dashed line) and the OmB standard deviation (solid line) for September 2021. Black line indicates all data and grey line quality screened data. The right panel shows the mean uncertainty with grey dashed line, OmB standard deviation with grey solid line and 0.75 x observed COD, used as observation error in the assimilation experiments, with black solid line.

Impact assessment in depleted observing system

To investigate the impact of the CCI AOD and COD from SLSTR instrument on model analysis and forecasts, to design optimal quality screening, and to test observation errors, extensive experiments with a depleted observing system have been performed with the IFS cycle 48R1 using the CAMS configuration. Experimentation in a depleted observing system is a common methodology used to emphasise the impact of adding a new instrument, channel or product into the assimilation system. In a depleted observing system, any changes can be attributed directly to the new added observations.

In these experiments, the “Baseline” experiment uses conventional observations (radiosonde, aircraft, synop, pilot, buoys) and GPS radio-occultation bending angles. It is considered to be a high-quality baseline, as it includes key components of the global observing system. AOD, COD or both are then added on top of the baseline configuration in different experiment configurations. Experiments are run over two periods, June 2020 and September 2021. As the



conclusions from both periods are similar, the results shown in this report focus on September 2021.

In all the experiments, AOD and COD observations are thinned to 0.5° spatial resolution, which is similar to operational thinning applied in AOD assimilation from other instruments. Also, both AOD and COD are actively assimilated only over sea. For AOD the decision is based on results from the passive monitoring presented in the previous section, over sea the data quality is high and more homogeneous than over land. For COD the decision is more practical, to limit the data amounts to manageable levels the ODB files only include data over sea and the quality over land was not assessed in the framework of this study.

The impact of the AOD assimilation has been assessed against AERONET data (Holben et al, 1998; Giles et al., 2019) using level 2.0 quality assessed measurements. Model data is interpolated to the observation sites. The performance is measured using the fractional gross error (FGE) and normalised mean bias (MNMB):

$$FGE = \frac{2}{n} \sum_{i=0}^n \left| \frac{AOD_i^m - AOD_i^o}{AOD_i^m + AOD_i^o} \right|$$
$$MNMB = \frac{2}{n} \sum_{i=0}^n \frac{AOD_i^m - AOD_i^o}{AOD_i^m + AOD_i^o}$$

These metrics are not sensitive for outliers in the distribution, and they range between $0 - 2$ and $-2 - 2$, respectively. In the equations n is the number of cases, AOD^m and AOD^o are the model and observed AOD, respectively.

Passive monitoring results for AOD indicate that the uncertainty estimate provided with the data has potential to be used as scene dependent observation error and the OmB standard deviation statistics are roughly two times larger in magnitude. Thus, as such the uncertainty is likely an underestimate of the optimal observation error. Sensitivity tests have been performed to decide which inflation factor to apply for the uncertainty estimate to obtain the best impact to the ECMWF system from assimilation of the AOD. The inflation factors tested were 1.0, 1.4, 2.0 and 3.0. Inflation factor 1.4 was suggested by the data providers based on their earlier investigations. In addition, constant observation error of 0.05 was included to the tests.

Figure 21 shows global average for the FGE for the different inflation factors over September 2021 (the observations are averaged over 12 hours). General conclusion is that adding the SLSTR AOD on top of the baseline experiment significantly improves the fit to the independent AERONET observations. The results indicate that 3 x uncertainty estimate is overestimate for observation error and the system benefits from giving more weigh for the AOD observations. However, using the uncertainty estimate as such is slightly underestimating the observation error. Impact difference between the other inflation factors is rather small and likely insignificant. It was decided to use inflation factor 1.4 in the joint assimilation experiments with COD.

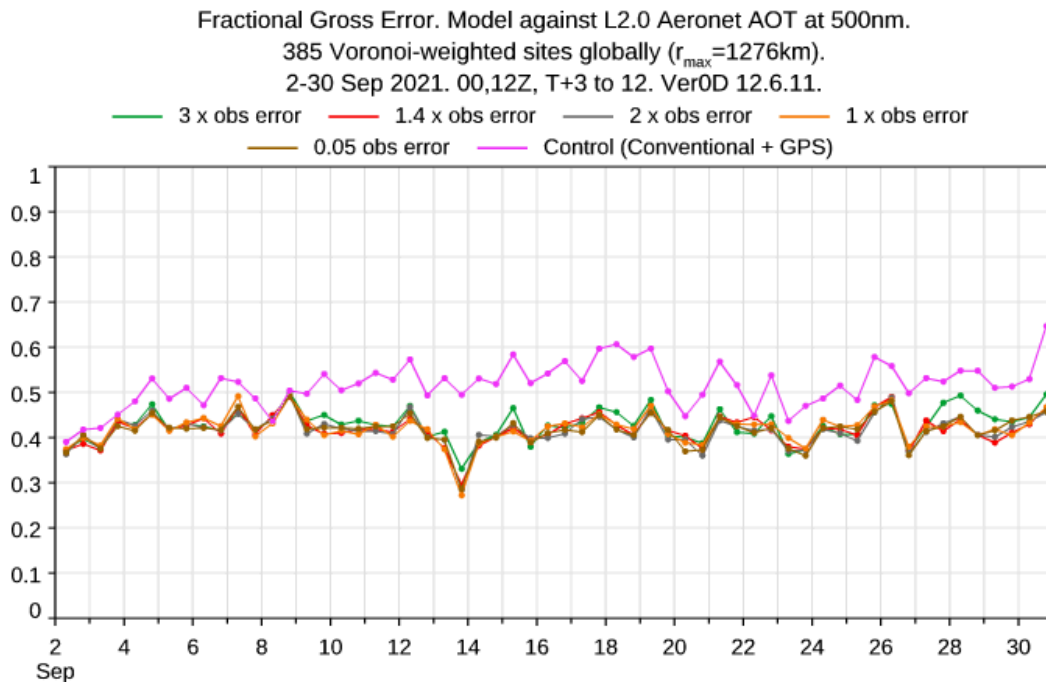


Figure 21: Global average of the fractional gross error (FGE) over September 2021. Magenta line indicates the Baseline experiment, green, grey, red and orange inflation factors 3, 2, 1.4 and 1 applied for uncertainty estimate to obtain observation error used in assimilation, respectively.

Sensitivity of the ECMWF system on assimilation of CODs was also tested in depleted observing system and with different configurations for the observation errors and data coverage. In earlier experimentations (A. Benedetti, personal communication) observation error 20% of the observed COD value has been used as observation error. This test was repeated as a first trial in the current system, as well as using 75% of the observed COD as indicated by the passive monitoring of the data. Using the uncertainty estimate provided with the data was not tested at this stage as it was over 5 times lower in magnitude than the OmB standard deviations.

Figure 22 shows the normalised change in the standard deviation of background differences for radiosonde observations for temperature (left panel) and specific humidity (right panel). The black line indicates experiment where the COD observation error is 20% of the observed value and the grey line experiment where the observation error is 75% of the observed value. In the forecast verification, values below 100% indicate improvement and over 100% degradation in the short-range forecast quality. The error bars indicate 95% confidence intervals. There is clear degradation in short range temperature forecasts also when the higher observation error is applied in assimilation. For short range humidity forecasts the impact becomes rather neutral when the observation error is increased from 20% to 75% of the observed COD value.

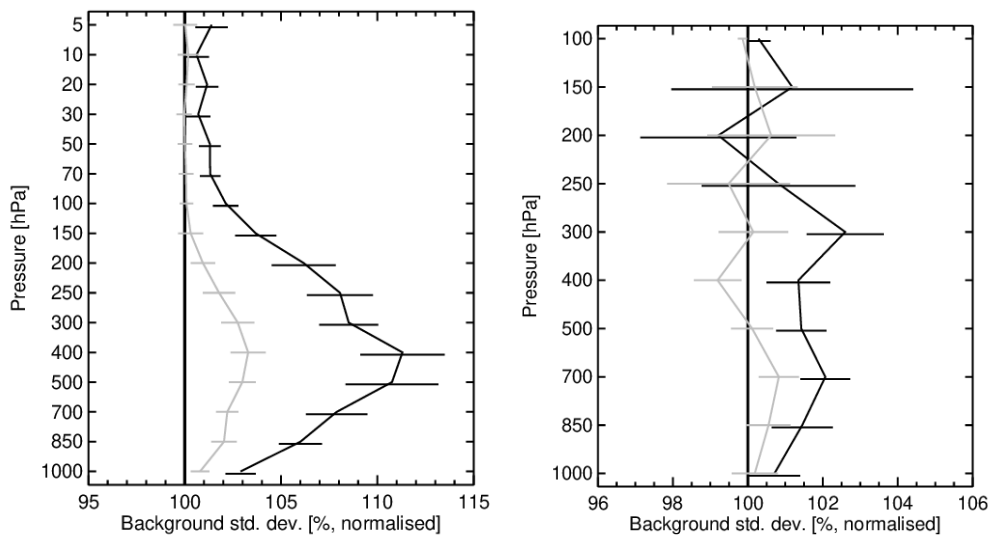


Figure 22: Normalised OmB standard deviation for radiosonde temperature (left panel) and specific humidity (right panel). The black line indicates the COD experiment using 20% of observed COD value as observation error, and the grey line experiment using 75% of observed COD value as observation error. 100% is the Baseline experiment. The period considered is September 2021.

Quality assessment of COD observations indicate that the largest biases (in magnitude and in geographical coverage) are seen over tropics. In these assimilation trials no variational bias correction has been implemented for COD, thus it is interesting to test if the impact could be improved either by blocklisting the data over tropics, or by limiting the COD values to the range 0.5 – 10 in order to exclude thick convective clouds where the observed and model COD can differ from each other notably. Figure 23 shows the impact on short range temperature (left panel) and humidity (right panel) forecasts but now the blue line indicates experiment where data over tropics is blocklisted and black line experiment where the observed COD values are restricted to be less than 10. With the restrictions which COD are active, the degradation in the temperature forecasts is significantly less, but it still is statistically significant degradation compared to the baseline forecast. For humidity the impact remains generally neutral.

For the joint test with AOD it was decided to use COD with global coverage but limited to the range of 0.5 – 10 and using 75% observed COD as observation error. Figure 24 shows the short-range impact on temperature (left) and humidity (right), black line indicating the COD assimilation only and grey line COD and AOD on top of the baseline experiment. The impact on short range temperature and humidity forecasts from the joint assimilation is rather neutral compared to the COD assimilation only. There is a slight hint of COD only performing better, but the differences are not statistically significant. Figure 25 shows the comparison of the impact compared to the AERONET AOD observations in terms of MNMB and FGE. Both metrics indicate that assimilation AOD or AOD + COD improve the fit to the independent observations. Assimilation of only AOD or both AOD and COD bring very similar impact to the system, with a small hint of AOD only performing slightly better. As with the temperature and humidity forecast verification, the differences are likely statistically insignificant.

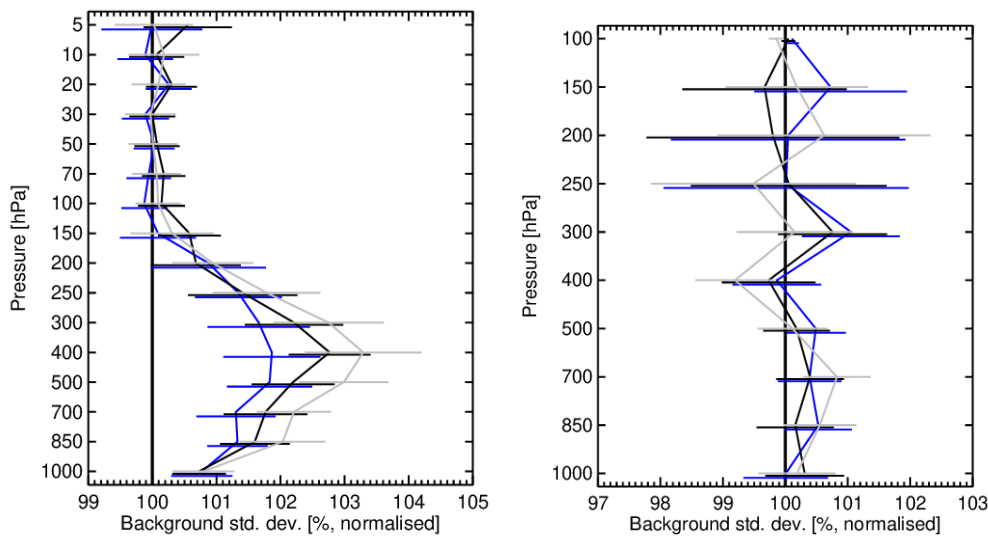


Figure 23: Similar to Figure 22 but grey line indicates experiment with all COD, black line indicates experiment where COD values are restricted to 0.5 – 10 and blue line experiment where COD is not used over the Tropics.

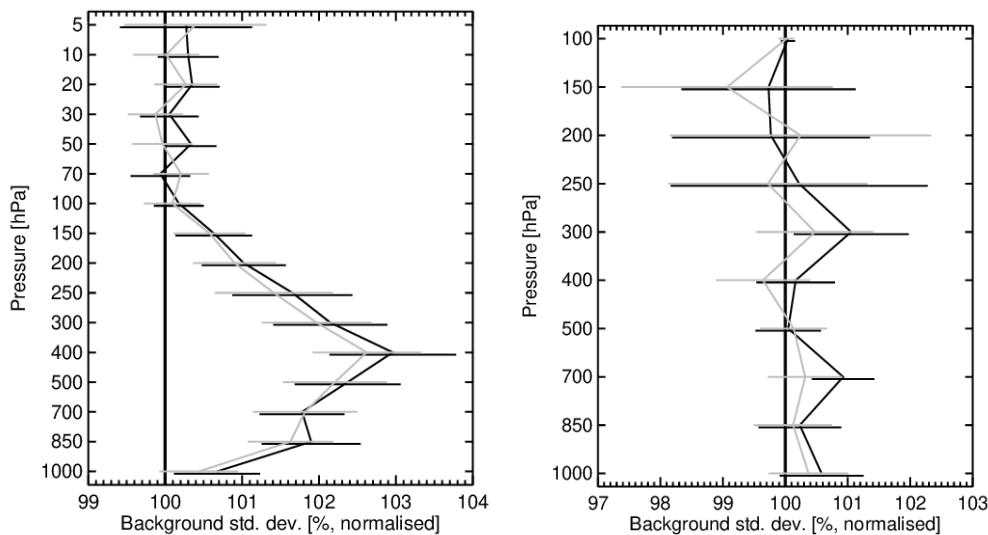


Figure 24: Similar to Figure 22 but black line indicates experiment with COD and AOD assimilated, and grey line experiment where only COD is assimilated on top of the baseline experiment.

Impact assessment in full observing system

Based on the several sensitivity experiments performed in the depleted observing system, the experimentation was repeated with the “optimal” set up in the full observing system. In summary this means using 1.4 x uncertainty estimate as observation error for AOD, 75% of

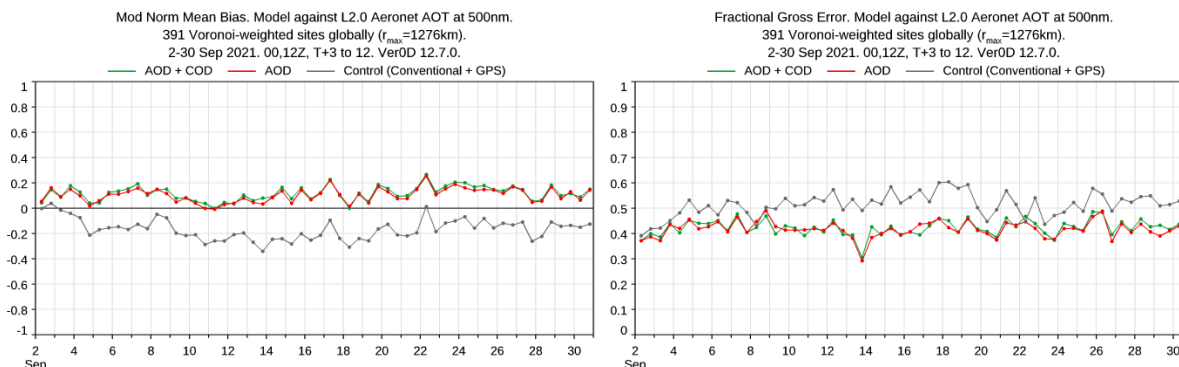


Figure 25: Global average of the normalised mean bias (MNMB, left panel) and fractional gross error (FGE, right panel) over September 2021. Green line indicates AOD + COD experiment, red line AOD experiment and grey line the baseline experiment.

observed COD value as observation error for COD and limiting the assimilated COD to the range of 0.5 – 10. Again, the experimentation was done over September 2021 and June 2020.

Left panel of Figure 26 shows the short-range forecast impact on temperature and humidity for September 2021. This time the verification is shown against ATMS instrument where channels 18 – 22 are sensitive to humidity and channels 6 – 15 to temperature at different altitudes of the atmosphere. There is clear degradation on temperature and humidity forecasts also in the full observing system. Verification against other satellite instruments (not shown) also support this conclusion. Verification against radiosonde observations is indicating also degradation for temperature forecasts but relatively neutral impact on humidity. However, there is clear positive signal for short-range wind forecasts as shown in the right panel of Figure 26. This can be a result of the tracer advection effect of the 4D-Var assimilation, e.g. wind fields can be changed to advect humidity to and from other areas. Results are very similar for June 2020 as shown in Figure 27 for humidity (left panel) and wind forecasts (right panel).

Verification against the AERONET observations indicates small benefits from assimilation of AOD and COD in the full observing system in terms of FGE which is shown in Figure 28 for September 2021 (left panel) and June 2020 (right panel).

Conclusions and recommendations

In the work package 5.5.2 the quality and impact of AOD and COD CCI products from SLSTR instrument have been assessed in the ECMWF system using the CAMS configuration. AOD data is v1.14 and COD based on v3.3, i.e. the COD data set used is not part of the official CCI data sets but same algorithms are used over the considered test periods.

Quality assessment with passive monitoring experiments, i.e. AOD or COD are not actively assimilated into the system, indicate high and homogeneous quality for the AOD observations over sea. For COD positive observation minus background mean differences are seen over areas where there is typically marine stratus clouds, and negative mean differences especially in the tropics where thick convective clouds are frequently present.

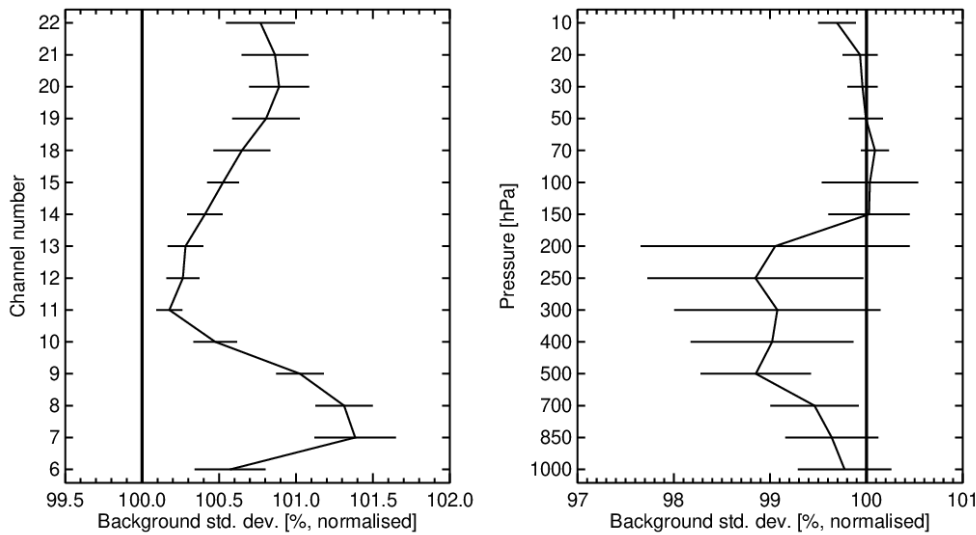


Figure 26: Similar to Figure 22 but black line indicates experiment with COD and AOD assimilated in full observing system. Left panel is verification against ATMS and right panel against conventional wind observations. Considered period is September 2021.

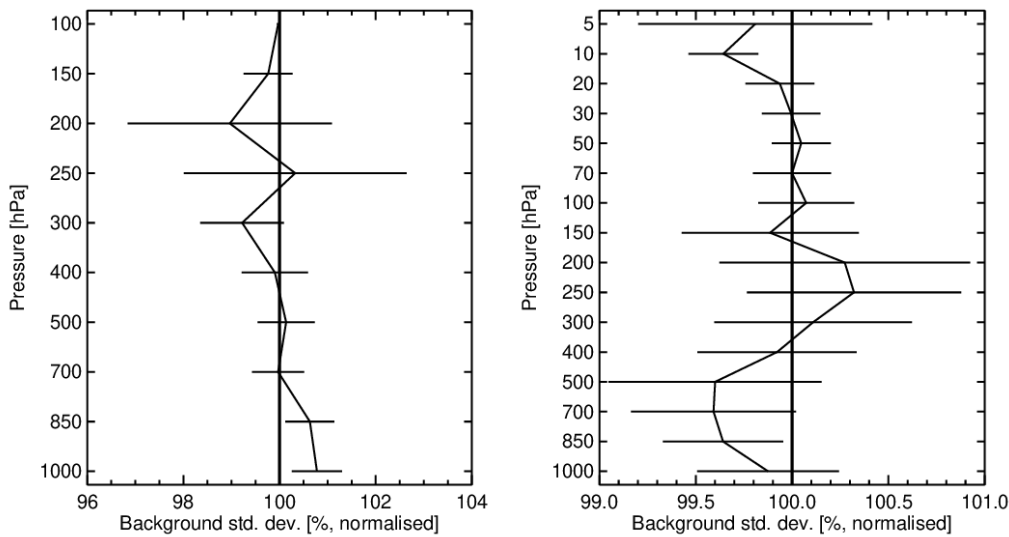


Figure 27: Similar to Figure 22 but black line indicates experiment with COD and AOD assimilated in full observing system. Left panel is verification against radiosonde humidity and right panel against conventional wind observations. Considered period is June 2020.

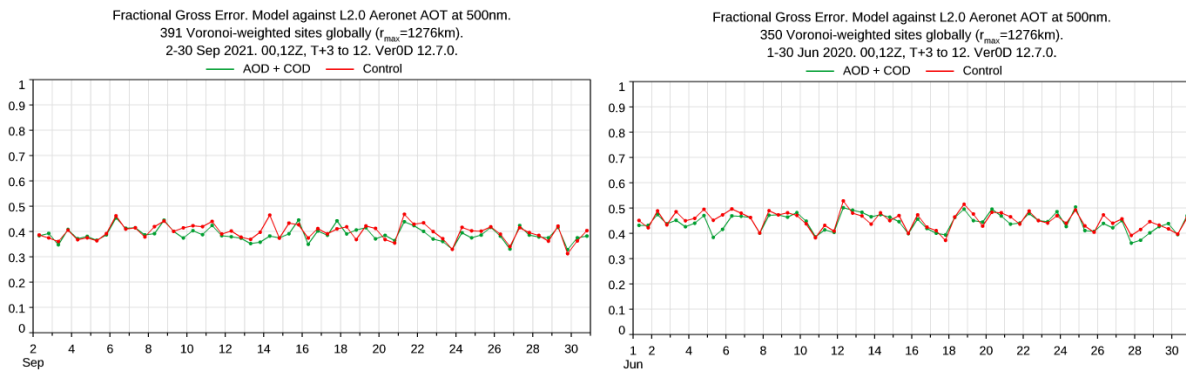


Figure 28: Global average of the fractional gross error (FGE) over September 2021 (left panel) and June 2020 (right panel). Green line indicates experiment where AOD and COD are assimilated in full observing system and the red line the baseline experiment.

The uncertainty estimate provided with AOD observations is sensible and can be used as scene dependent observation error in the assimilation with slight inflation. Sensitivity tests suggest inflation factor of 1.4 to be a reasonable choice. The uncertainty estimate provided with the COD observations is low in magnitude compared to the corresponding OmB standard deviation statistics. For quality screened data the OmB standard deviation statistics are still indicating magnitude of six times larger than the uncertainty estimate. Thus, in the first assimilation trials the observation error was simply calculated as a percentage of the observed COD value, and value 75% was chosen due to the good fit to the OmB statistics. Due to limited time available within the project, no variational bias correction was implemented for COD, instead some sensitivity tests were performed with excluding data over tropics or with high COD values which indicate deep convective situations.

Impact assessment has been performed in depleted and in full observing system. Depleted system was used in the sensitivity tests and the final optimal configuration of joint AOD and COD assimilation was then tested in the full observing system framework. Both experiment configurations indicate degradation in temperature and humidity forecasts. However some positive signal is seen for wind forecasts which can be due to the tracer advection effect of the 4D-Var assimilation. Verification against the AERONET observations indicate small but positive signal from assimilation of the CCI AOD and COD.

There are several suggestions how the impact of the COD assimilation could be improved from these first trials. First, the quality screening of the data could be made stricter. In these experiments we did not perform sensitivity tests with the first guess check where the observed value is compared to the model counterpart and rejected if they deviate too much. Second, the monitoring statistics indicate significant biases over some areas. Thus, implementing variational bias correction for the COD assimilation could be beneficial. Third, developing more sophisticated observation error model could be beneficial.

The results show that the CCI AOD product is mature and behaves in a similar way in the ECMWF system than the operationally used AOD products from other instruments. As a recommendation to the data providers, we only suggest to continue the close dialogue and co-operation with the data users.

CMUG CCI+ Deliverable

Reference: Final report WP5.5: Cloud and Aerosol Analysis Study
Due date: August 2024
Submission date: September 2024
Version: 0.4



The COD product was tested in assimilation for the first time. Thus, no similar maturity can be expected as that of the AOD product. We would suggest focusing on developing further the quality information provided with the data. This includes both the uncertainty estimates which in our understanding are significantly too low in the current version, and the quality flags which now only screen out very few observations and do not improve the fit to the model background. If the COD product is aimed for operational assimilation, also discussions of the data format would be useful. Global observation files covering 24 hours are not optimal without pre-processing in any operational assimilation system as the assimilation windows are typically much shorter.

Overall conclusion is that the main benefits of projects like this is to have the fruitful two-way conversation between the data providers and data users.



References

- Adebisi, A., J.F. Kok, B.J. Murray, C.L. Ryder, J.-B.W. Stuut, R.A. Kahn, P. Knippertz, P. Formenti, N.M. Mahowald, C.P. García-Pando, M. Klose, A. Ansmann, B.H. Samset, A. Ito, Y. Balkanski, C. Di Biagio, M.N. Romanias, Y. Huang, J. Meng. A review of coarse mineral dust in the earth system *Aeolian Res.*, 60 (2023), Article 100849, [10.1016/j.aeolia.2022.100849](https://doi.org/10.1016/j.aeolia.2022.100849)
- Amiridis, V., Marinou, E., Tsekeri, A., Wandinger, U., Schwarz, A., Giannakaki, E., Mamouri, R., Kokkalis, P., Biniotoglou, I., Solomos, S., Herekakis, T., Kazadzis, S., Gerasopoulos, E., Proestakis, E., Kottas, M., Balis, D., Papayannis, A., Kontoes, C., Kourtidis, K., Papagiannopoulos, N., Mona, L., Pappalardo, G., Le Rille, O., and Ansmann, A.: LIVAS: a 3-D multi-wavelength aerosol/cloud database based on CALIPSO and EARLINET, *Atmos. Chem. Phys.*, 15, 7127–7153, <https://doi.org/10.5194/acp-15-7127-2015>, 2015
- Benedetti, A., and Janiskova, M.: Assimilation of MODIS cloud optical depths in the ECMWF model. *Monthly Weather Review - MON WEATHER REV.* 136. [10.1175/2007MWR2240.1](https://doi.org/10.1175/2007MWR2240.1), 2008.
- Benedetti, A., Morcrette, J.-J., Boucher, O., Dethof, A., Engelen, R., Fisher, M., Flentje, H., Huneus, N., Jones, L., Kaiser, J., Kinne, S., Mangold, A., Razinger, M., Simmons, A. J., and Suttie, M.: Aerosol analysis and forecast in the European centre for medium-range weather forecasts integrated forecast system: 2. Data assimilation, *J. Geophys. Res.-Atmos.*, 114, D13205, <https://doi.org/10.1029/2008JD011235>, 2009.
- Desroziers, G., L. Berre, B. Chapnik, and P. Poli: Diagnosis of observation, background and analysis-error statistics in observation space. *Quart. J. Roy. Meteor. Soc.*, 131, 3385–3396, <https://doi.org/10.1256/qj.05.108>, 2005.
- Di Tomaso, E., Escribano, J., Basart, S., Ginoux, P., Macchia, F., Barnaba, F., Benincasa, F., Bretonnière, P.-A., Buñuel, A., Castrillo, M., Cuevas, E., Formenti, P., Gonçalves, M., Jorba, O., Klose, M., Mona, L., Montané Pinto, G., Mytilinaios, M., Obiso, V., Olid, M., Schutgens, N., Votsis, A., Werner, E., and Pérez García-Pando, C.: The MONARCH high-resolution reanalysis of desert dust aerosol over Northern Africa, the Middle East and Europe (2007–2016), *Earth Syst. Sci. Data*, 14, 2785–2816, <https://doi.org/10.5194/essd-14-2785-2022>, 2022.
- Escribano, J., Di Tomaso, E., Jorba, O., Klose, M., Gonçalves Ageitos, M., Macchia, F., Amiridis, V., Baars, H., Marinou, E., Proestakis, E., Urbanneck, C., Althausen, D., Bühl, J., Mamouri, R.-E., and Pérez García-Pando, C.: Assimilating spaceborne lidar dust extinction can improve dust forecasts, *Atmos. Chem. Phys.*, 22, 535–560, <https://doi.org/10.5194/acp-22-535-2022>, 2022.
- Giles, D. M., Sinyuk, A., Sorokin, M. G., Schafer, J. S., Smirnov, A., Slutsker, I., Eck, T. F., Holben, B. N., Lewis, J. R., Campbell, J. R., Welton, E. J., Korkin, S. V., and Lyapustin, A. I.: Advancements in the Aerosol Robotic Network (AERONET) Version 3 database – automated near-real-time quality control algorithm with improved cloud screening for Sun photometer aerosol optical depth (AOD) measurements, *Atmos. Meas. Tech.*, 12, 169–209, <https://doi.org/10.5194/amt-12-169-2019>, 2019.
- Holben, B. N., Eck, T. F., Slutsker, I., Tanre, D., Buis, J. P., Setzer, A., Vermote, E., Reagan, J. A., Kaufman, Y., Nakajima, T., Lavenue, F., Jankowiak, I., and Smirnov, A.: AERONET – A federated instrument network and data archive for aerosol characterization, *Remote Sens. Environ.*, 66, 1–16, [https://doi.org/10.1016/S0034-4257\(98\)00031-5](https://doi.org/10.1016/S0034-4257(98)00031-5), 1998.
- Hunt, B. R., Kostelich, E. J., and Szunyogh, I.: Efficient data assimilation for spatiotemporal chaos: A local ensemble transform Kalman filter, *Physica D*, 230, 112–126, <https://doi.org/10.1016/j.physd.2006.11.008>, 2007.

CMUG CCI+ Deliverable

Reference: Final report WP5.5: Cloud and Aerosol Analysis Study
Due date: August 2024
Submission date: September 2024
Version: 0.4



Klose, M., Jorba, O., Gonçalves Ageitos, M., Escibano, J., Dawson, M. L., Obiso, V., Di Tomaso, E., Basart, S., Montané Pinto, G., Macchia, F., Ginoux, P., Guerschman, J., Prigent, C., Huang, Y., Kok, J. F., Miller, R. L., and Pérez García-Pando, C.: Mineral dust cycle in the Multiscale Online Nonhydrostatic Atmosphere Chemistry model (MONARCH) Version 2.0, *Geosci. Model Dev.*, 14, 6403–6444, <https://doi.org/10.5194/gmd-14-6403-2021>, 2021.

Pu, B., and Ginoux, P.: The impact of the Pacific Decadal Oscillation on springtime dust activity in Syria, *Atmospheric Chemistry and Physics*, 16(21), 13431-13448, 2016.